Partial Discharge Detection and Localization in High Voltage Transformers Using an Optical Acoustic Sensor

by

Alison K. Lazarevich

Thesis submitted to the faculty of

the Virginia Polytechnic Institute and State University

in partial fulfillment of the requirements for the degree of

Master of Science

in

Electrical Engineering

Approved By:

Dr. Anbo Wang, Committee Chair

Dr. Yilu Liu, Committee Member

Dr. Wayne Scales, Committee Member

May 12, 2003
Blacksburg, Virginia
U.S.A.

Keywords: Partial Discharge (PD), High Voltage Transformer (HVT), Acoustic Emission, Fiber Optic Acoustic Sensor, Time Difference of Arrival (TDOA), Hyperbolic Positioning

Partial Discharge Detection and Localization in High Voltage Transformers Using an Optical Acoustic Sensor

by
Alison K. Lazarevich

ABSTRACT

A partial discharge (PD) is the dissipation of energy caused by the buildup of localized electric field intensity. In high voltage devices such as transformers, this buildup of charge and its release can be symptomatic of problems associated with aging, such as floating components and insulation breakdown. This is why PD detection is used in power systems to monitor the state of health of high voltage transformers. If such problems are not detected and repaired, the strength and frequency of PDs increases and eventually leads to the catastrophic failure of the transformer, which can cause external equipment damage, fires and loss of revenue due to an unscheduled outage. Reliable online PD detection is a critical need for power companies to improve personnel safety and decrease the potential for loss of service.

The PD phenomenon is manifested in a variety of physically observable signals including electric and acoustic pulses and is currently detected using a host of exterior measurement techniques. These techniques include electrical lead tapping and piezoelectric transducer (PZT) based acoustic detection. Many modern systems use a combination of these techniques because electrical detection is an older and proven technology and acoustic detection allows for the source to be located when several sensors are mounted to the exterior of the tank. However, if an acoustic sensor could be placed inside the tank, not only would acoustic detection be easier due to the increased signal amplitude and elimination of multipath interference, but positioning could also be performed with more accuracy in a shorter time.

This thesis presents a fiber optic acoustic sensing system design that can be used to detect and locate PD sources within a high voltage transformer. The system is based on an optical acoustic (OA) sensor that is capable of surviving the harsh environment of the transformer interior while not compromising the transformer's functionality, which allows for online detection and positioning. This thesis presents the theoretical functionality and experimental validation of a band-limited OA sensor with a usable range of 100-300 kHz, which is consistent with the frequency content of an acoustic pulse caused by a PD event. It also presents a positioning system using the time difference of arrival (TDOA) of the acoustic pulse

with respect to four sensors that is capable of reporting the three-dimensional position of a PD to within ±5cm on any axis.

This work was supported in part by NSF grant 9810688.

Acknowledgements

I would like to thank Dr. Anbo Wang for bringing me to the Center for Photonics Technology and giving me this wonderful project. I would also like to thank him for being my academic advisor and showing such confidence in my abilities and encouraging me to perform to the best of my capabilities.

I would also like to thank Dr. Yilu Liu and Dr. Wayne Scales for agreeing to be on my defense committee and offering their expertise to make the results of this project as accurate and successful as possible.

To the members of the CPT staff, I would like to extend my sincere gratitude. Thank you to Dr. Kristie Cooper for her guidance, advice and without whom, this document and my success as a research assistant would not have been possible. Also, to Ms. Debbie Collins, thank you for all of the administrative support as well as personal advice. You gave your help so selflessly and I will always remember to your kindnesses. Finally, thank you to the students of the CPT for your help and support, especially Bing Yu for your knowledge and DaeWoong Kim for your patience.

To Dr. William Baumann and Dr. Timothy Pratt, thank you for the wisdom you shared with me both inside and outside the classroom. You both have seen me grow academically and personally and I thank you for all of the wonderful advice that has shaped me into the professional I am today.

I would also like to thank my friends and family who kept me sane during my Masters studies. To Michael Carr, thank you for always being there and for being so understanding during my late lab hours and long nights of writing. You are my inspiration and my joy. To my friends, Colleen Shannon, Mark Bucciero, Nancy Bahrami, Mandy Cundy, Edric Carter and Jessica Armstrong, thank you for the love and support and general good humor you have given so freely over the last year and a half. To my parents, Mio and Alyce, thank you for pushing me to discover my true potential and teaching me the importance of respect for ones self as well as for others. Finally, to God I am eternally indebted for the talents you have given me and the good fortune I have been afforded. I hope that I may use my knowledge to make the world a more fulfilling and peaceful place.

Table of Contents

List of Figures

List of Tables

Chapter 1: Introduction

Section 1.1: Overview

A partial discharge (PD) is short release of current caused by the buildup of electric field intensity in a finite region. In high voltage devices, such as transformers, PDs can be symptomatic of problems within the device such as floating components and insulation flaws. When a transformer is first manufactured, PD detection can be used as a tool to judge the state of the device and the quality of its manufacture. In addition, as the transformer ages, faults in the device can be created. Over time, electrical and mechanical stresses can damage materials within the transformer, including the winding and the paper insulation lining the walls of the transformer tank. If the damage is not detected or corrected, the faults can cause the transformer to operate outside of its normal parameters and eventually a catastrophic failure will occur, causing potential damage to surrounding equipment and facilities, as well as lost revenue due to an unscheduled power outage [1]. In a modern high voltage power system, PD detection is used to monitor the state of health of a transformer in service and helps plant managers schedule device maintenance.

The primary methods of PD detection are based on the observable electric and acoustic characteristics of the phenomenon. Acoustic PD detection systems are more favorable than electric systems in transformer monitoring because in addition to detection, measurement of the observed PD signal by several acoustic sensors allows for PD location [2]. Position information can then be used by plant monitors to diagnose the cause of the PD as well as shorten maintenance time. The problem with current acoustic PD detection systems is that the acoustic signal must be observed outside of the transformer tank because there are no developed sensors that can survive the environment of the tank interior and be electrically and chemically neutral. Because the path between a PD and the acoustic sensors includes the wall of the tank, multipath interference can severely limit the accuracy of any positioning system. The interference is caused by the differing acoustic velocity of the wave in the mineral oil and the transformer tank. As the acoustic pulse travels away from the source, it encounters the tank wall at different times and then is recorded by the exterior sensor. In the case of the HVT, the path that travels through the tank walls reaches the sensor before the direct path through the oil because the acoustic velocity in steel is much higher than mineral oil. This transit time discrepancy can lead to pulse distortion that leads to an erroneous TDOA calculation. Therefore, it would be an enormous advantage if a sensor could be designed to operate within the transformer tank without inhibiting or changing the functionality of the transformer [3]. Once an internal sensor has been designed, a positioning system must be employed that makes the most efficient use of the captured acoustic signals. The location of the source of the PD within the transformer tank is determined by measuring the time difference of arrival (TDOA) of the acoustic signal between each of several sensor positions within the tank, which can then be used to solve a system of non-linear equations [4].

This thesis presents an optical based sensor system that has both acoustic detection and source location capabilities. The sensor, a fiber optic acoustic sensor based on extrinsic Fabry-Perot interferometry (EFPI), is made of silica so that it is both chemically and electrically inert and can survive the harsh environment of the transformer interior without compromising or altering the functionality of the device. This allows for the sensors to record data while the transformer is online so that the HVT can be monitored constantly and no loss of service is necessary. The system also has positioning capabilities because it consists of four sensors, which provide three TDOA measurements and can provide the source position in three dimensions with an accuracy bounded by a 10cm cube.

The development of this system is important because current PD detection and location systems are insufficient to provide reliable results in a reasonable amount of time. In the case of electrical or chemical detection, which is outlined in Chapter 2, position information is all but impossible to obtain using those methods alone. Acoustic detection offers the ability to locate a PD event, but current systems quote accuracies of between 10cm on each axis [5] and a foot [2] and require computationally expensive algorithms and periods of observation in the order of hours to find a single PD source location [6]. The system presented in this thesis has the potential to allow for real time detection and positioning at accuracies surpassing those found in the literature.

Section 1.2: Contributions to the Field

This research project contributes to the field of PD detection and location in the following ways.

1. Provides a detailed description of the frequency response of an optical acoustic sensor. This description also includes an algorithm for the processing of the frequency response results to yield a meaningful curve for the response of this particular sensor that can be used to evaluate the viability of using the sensor for different applications.

2. Details a positioning algorithm that can be used to position a PD event within an acoustic medium using a direct measurement of the acoustic field.

3. Analyzes the sources of error that can affect the positioning of a PD event. These error sources include time resolution of the data, pulse time separation between sensors, center frequency of the PD acoustic pulse, and signal to noise ratio of the captured acoustic signal. This analysis is based on both simulated and experimental data.

Section 1.3: Organization of the Thesis

This thesis is organized into five chapters as follows.

Chapter 1: Introduction to the project as well as the motivation behind the investigation of PD detection and location.

Chapter 2: Background covering the field of partial discharges, their physical manifestations, and current methods of detection and positioning. This chapter also covers the benefits and problems associated with different PD detection methods as well as the reasoning for using acoustic detection.

Chapter 3: Theory and test data associated with the optical acoustic EFPI sensor to be used in the detection and location system. The chapter gives a detailed description of the functionality of the sensor as well as design considerations for PD detection. The final part of the chapter presents experimental results that validate the primary theoretical design parameters for the sensor, namely frequency response.

Chapter 4: Theoretical and test data associated with the chosen positioning system. The first part of the chapter outlines the positioning algorithm to be used for PD location as well as simulation data that validates the selection of hyperbolic difference as a method of position determination. The second half of the chapter presents experimental data taken at different points in the test set up and the resulting position accuracy.

Chapter 5: Conclusions from the study. This chapter also includes areas of future research that would allow this sensor system to be deployed in the commercial power industry.

Section 1.4: References

[1] H. X. Jiangdong Deng, Wei Huo, Ming Luo, Russ May, Anbo Wang, and Yilu Liu, "Optical fiber sensor-based detection of partial discharges in power transformers," *Optics and Laser Technology*, vol. 33, pp. 305-311, 2001.

[2] P. M. Eleftherion, "Partial Discharge XXI: Acoustic Emission-Based PD Source Location in Transformers," in *IEEE Electrical Insulation Magazine*, vol. 11, 1995, pp. 22-26.

[3] A. Z. a. T. R. Blackburn, "Acoustic Detection of Partial Discharges Using Non-Intrusive Optical Fibre Sensors," presented at IEEE International Conference on Condition and Breakdown in Solid Dielectrics, Vasteras, Sweden, 1998.

[4] Y. T. a. H. Chan, K.C., "A Simple and Efficient Estimator for Hyperbolic Location," *IEEE Transactions on Signal Processing*, vol. 42, pp. 1905-1915, 1994.

[5] V. Darley, "Partial Discharges within Power Transformers and the Use of Ultrasonic Techniques in Their Location," presented at IEE Colloquium on Assessment of Degradation Within Transformer Insulation Systems, London, U.K., 1991.

[6] I. J. Kemp, "Partial discharge plant-monitoring technology: Present and future developments," *IEE Proc.-Sci. Meas. Technology*, vol. 142, pp. 4-10, 1995.

Chapter 2: Background

Partial Discharge (PD) detection is an important tool for monitoring insulation conditions in high voltage (HV) devices in power systems. As the HV device ages, the insulation can breakdown due to mechanical, thermal and electrical stress, resulting in the catastrophic failure of the device. Therefore it is important to have a system that is capable of warning device users of potential insulation problems so that they may be repaired during a scheduled shutdown. In order to design a system to detect and locate this phenomenon within an HV transformer, it is important to understand why PDs occur and what methods are currently employed to detect and locate PDs.

Section 2.1: Partial Discharge

A partial discharge in an HV transformer (HVT) occurs when the electric field in a localized area changes in such a way that a localized current is created. This localized current manifests itself as an electrical pulse that is measurable at the output of the transformer. The most likely sources of PDs can be broken down into three categories: floating components, coronas, and voids. Information on the importance and mechanisms of floating components and coronas in HV transformers can be found in Ref [1]. However, the detection of PDs created by these two sources does not yield any useful information about the insulation because their appearance is not directly related to the condition of the insulation. Insulation breakdown is physically manifested as small cracks, *i.e.* voids, in the insulation; therefore, only void sources will be considered here.

Voids are defined as gaps in a more dense dielectric material, such as gas bubbles in oil that fills the transformer tank, or cracks and fissures in the paper insulation lining the transformer walls. The void region has a lower dielectric constant than the surrounding material, creating a capacitance. A partial discharge can then occur when the electric field difference across the void exceeds minimum breakdown field strength [1]. However, reaching this minimum field strength does not guarantee an immediate partial discharge. In order for a PD to occur, two criteria must be met. First, the electric field difference across the void must be higher than the breakdown value, which is determined by the field's ability to accelerate an electron to the point that if it impacts another molecule, more electrons are knocked loose than are absorbed. Second, there must be a free electron present within a specific volume, whose size is proportional to the voltage across the void, to accelerate within the field. If these conditions are met, then the buildup of electrons in motion grows exponentially and a streamer, or electron channel, is created and current can flow across the void and return the voltage across the void to zero*. However, the presence and location of a free electron is a random process dominated by the presence of ambient radiation knocking electrons loose from surrounding materials. Even the largest source of ambient radiation in most systems, cosmic rays, creates very few free electrons.

In summary, in order for a PD to occur, a free electron must be present within a voltage dependent volume while the electric field strength is high enough to cause a cascading flow of electrons from the movement of a single free accelerated electron. This need for free electrons makes the PD phenomenon very unpredictable and a PD can occur within minutes or within hours of reaching the breakdown field strength within the void [2]. The resulting discharge manifests itself as an observable electrical, acoustic, and sometimes optical signal. It should be noted at this time that the exact mechanisms and resulting signal properties of a partial discharge are not completely understood, though there are loose guidelines that device designers can use in building detection systems [3].

Section 2.2: Detection Methods

Over time, the insulation within an HVT begins to breakdown due to mechanical, thermal and electrical stress. Because partial discharges are both symptomatic of insulation breakdown and a mechanism for further insulation damage, PD detection is used to evaluate the condition of and diagnose problems with the HVT insulation [4]. Over the past forty years, several methods have been developed to detect PDs within HVTs. These can be grouped into four categories, based on the PD manifestation that they measure: chemical, electrical, acoustic and optical detection. Optical detection is not widely used in current systems and is difficult to implement in HVTs due to the opaque nature of mineral oil. The remaining three techniques are described in this section.

* The potential across the void does not actually return to zero. But for the purposes of this paper, this assumption can be made to illustrate how the process works.

Section 2.2.1: Chemical Detection

Partial discharges can be detected chemically because the current streamer across the void can break down the surrounding materials into different chemical components. The two primary chemical tests employed by power companies today are dissolved gas analysis (DGA) and high performance liquid chromatography (HPLC). The DGA test identifies gas levels in the oil produced by the breakdown of mineral oil in the transformer into different gases, which dissolve back into the oil. The test is administered by taking an oil sample from the tank and determining the levels of different dissolved gases, which include acetylene, methane, hydrogen, carbon dioxide, and ethylene [3]. This test indicates the presence of PDs as well as provides additional diagnostic information because different levels of each of the gases can be correlated to a specific type of fault within the HVT using extensively developed tables. Although this test is widely used, there is some debate as to whether or not the levels of dissolved gas really correlate to a specific type of fault. Some experts argue that the rate of increase of these gases is more important than the absolute measure of their concentration [5].

Another test, HPLC, measures the byproducts of transformer wall insulation breakdown. Because the insulation on the wall of the transformer is made of paper, the breakdown products are glucose and degraded forms of glucose. The test is administered by evaluating oil samples from the transformer in an offsite lab. However, there are problems with this test as well. The glucose levels in the oil are very small because glucose is not highly soluble in mineral oil and the degraded forms of glucose are not very stable. In addition, this test suffers the same uncertainty as DGA because there are no standard values for glucose concentration and their correlation to HVT faults [3].

Chemical testing has some limitations that prevent it from being the only method used for PD detection. First, chemical testing does not provide any information about the position of the PD or the extent of the insulation damage. However, further research is being conducted to add chemical "tags" to transformer insulation that would be released and dissolved into the oil in the event of a PD. If these tags could be manufactured and implemented into new transformer insulations, then HPLC could provide valuable information about the type of PD fault that has occurred within the transformer. However, this does not satisfy the need to elicit position information from chemical PD detection. The second problem is that chemical testing cannot be performed online. In most cases, the transformers must be taken out of operation to obtain the oil sample. In the case of HPLC, the oil sample must be sent outside of the HVT site in order to be analyzed and results can take a long time to obtain. These problems limit the usefulness of chemical detection and rule it out as a singular solution to PD detection and positioning.

Section 2.2.2: Electrical Detection

Electrical detection focuses on capturing the electrical pulse created by the current streamer in the void. These pulses last on the order of single nanoseconds and have measurable frequency components in excess of 1 MHz [1]. The pulse shape, its relative phase location within the AC cycle of the HVT, and the signal intensity all lead to information about the type of PD fault and the severity of the insulation damage. Electrical measurements are grouped into two categories, direct probing and RF emission testing. The direct probing method requires that capacitive couplers be connected to the phase terminals of the transformer. The second group, RF emission testing, is conducted by using antennas in the area of the transformer. Both methods require a time domain recording device, such as a data storage oscilloscope, to capture the PD signal. The PD is then identified using several digital processing methods. These processing methods make online electrical PD detection very attractive because it makes real-time monitoring of HV systems possible.

Like chemical detection, electrical detection has limitations. The primary limitation of electrical testing is its susceptibility to noise. The HVT environment contains high levels of electrical noise, both narrowband and broadband. In some cases, it is extremely difficult to distinguish between noise and a PD because of the short PD pulse width. This problem leads to false detection in online electrical PD systems. The transformer can be taken offline and connected to an external power source for testing in order to eliminate some of the noise, but taking the HVT offline can cost hundreds of thousands of dollars a day in lost revenue for the power company [4]. Another problem with electrical detection is that the received pulse characteristics are highly dependent on the geometry of the HVT. Different components within the transformer can distort the pulse shape needed to characterize the type of PD fault and can again result in erroneous detection. Although electrical detection has several problems, these systems are widely used in power plants around the world and provide equipment managers with valuable information about the condition of the HVT [3].

Section 2.2.3: Acoustic Detection

Acoustic detection, like electrical detection, focuses on the acquisition and recording of a signal generated by a partial discharge. However, instead of capturing an electrical signal, acoustic PD detection endeavors to sense and record the acoustic signal created during a PD event. This signal is created because when the current streamer is formed within the void, the material around the hot streamer is vaporized. This vaporization causes an explosion of mechanical energy, which then propagates through the transformer tank in the form of a pressure field [6]. This phenomenon is analogous to the formation of thunder after a lightning strike.

Acoustic detection is widely used in HVTs as well as gas insulated substations (GIS). Systems employing this method can be broken into two categories: external systems and internal systems. External acoustic detection systems, which are currently more widely utilized in power systems, employ sensors mounted to the outside of the transformer tank to detect the PD acoustic signal. Conversely, internal systems use sensors placed inside the transformer tank to directly measure the pressure wave in the mineral oil. Systems utilizing each method will be discussed in more detail in the next section.

The primary advantage of using acoustic detection over chemical and electrical methods is that position information is readily available from acoustic systems using sensors at multiple locations. This position information can help to identify the type of PD as well as the location and severity of an insulation fault. The position information can also help plant technicians locate faults in insulation for repair purposes. Another advantage of acoustic detection over electrical detection is its immunity to electromagnetic interference (EMI). This immunity to EMI makes acoustic detection ideal for online PD detection because a better signal to noise ratio (SNR) for the acoustic signal will lead to fewer false alarms. However, immunity to EMI does not mean that there is no acoustic noise in the system. Mechanical vibrations in the transformer core are the primary source of acoustic noise, but the frequency content of these vibrations are sufficiently lower than the PD acoustic signal.

Acoustic detection also has its limitations. The primary problem with acoustic detection is the complex nature of the acoustic wave propagation. Because HVTs are not homogeneous devices, the waves do not travel in perfect spherical wavefronts[†]. The wavefront suffers from

---

[†] Because the source of PD is so small, it can be seen as an acoustic point source. Due to the nature of wave propagation, point sources lead to spherical wave fronts.

reflection off of objects within the tank, which can lead to multipath noise and diminished signal strength, and is also perturbed by dispersion and absorption in the mineral oil. Another difficulty with acoustic detection is the required sensitivity. Classically, due to the many attenuation mechanisms, received acoustic signals have very low intensity and so sensors must be very responsive to small changes in signal amplitude in order to detect a PD [3].

Section 2.3: Acoustic Detection Systems

The remaining chapters of this thesis describe the design and implementation of a fiber optic acoustic detection system. This section provides the necessary review of acoustic signal propagation and acoustic detection systems currently in production.

Section 2.3.1: Acoustic Wave Propagation

Although the mechanisms of propagation are different for acoustic waves and electromagnetic waves, the mathematics that describes both conditions is very similar. To find the pressure field created by an acoustic wave, one must solve a second order differential equation of the form

$$\nabla^2 p = \frac{1}{c^2}\frac{\partial^2 p}{\partial t^2} \qquad \textit{(Eq. 2.1)}$$

where p is the pressure field, ∇^2 is the scalar Laplacian operator, and c is the speed of sound in the medium of interest [6]. This equation is of the same form as the scalar wave equation in electromagnetics if the scalar quantity p is replaced by either e for the electric field or h for the magnetic field. Therefore, knowledge about one subject can be used to gain insight into the other. Since a PD is seen as an acoustic point source, the resulting acoustic waves in the liquid medium of the transformer tank will be spherical [7]. In addition, the acoustic pulse will suffer from dispersion and absorption due to the properties of the mineral oil. Finally, the waves will suffer from constructive and destructive interference at the boundaries of the tank because the acoustic impedance of the two materials, steel and mineral oil, are different. These basic facts about acoustic propagation are sufficient to explain the fundamental problems and benefits associated with acoustic detection.

Section 2.3.2: Current Systems

Acoustic detection systems, as mentioned above, can be grouped into external and internal systems. External systems employ acoustic sensors located outside of the transformer tank. Several different technologies are used to fabricate these external sensors, but piezoelectric transducers based on ferroelectric ceramic materials such as lead zirconium titanate (PZT) dominate the systems currently in use. A PZT converts acoustic energy into an electrical signal. Two types are used in acoustic detection, accelerometers and acoustic emission sensors. Accelerometers, which have a useful frequency range of up to 50 kHz, produce an electrical signal that is proportional to the acceleration of the surface that the sensor is connected to. In contrast, acoustic emission sensors, with a frequency range between 30 kHz and 1 MHz, produce an electrical signal that is proportional to the velocity of the contact surface [7]. Figure 2.1 illustrates the typical frequency response of each sensor type.

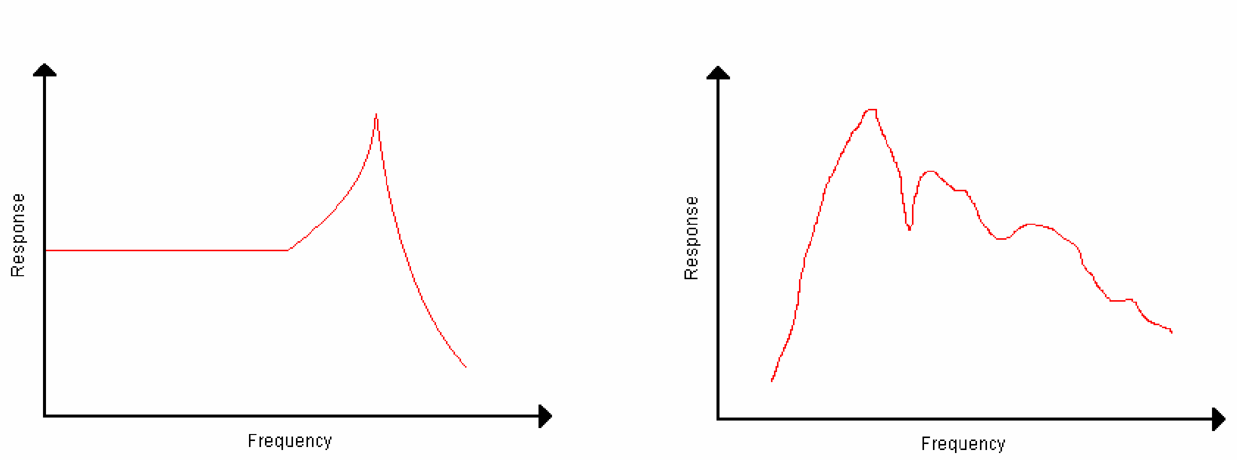

Figure 2.1: Illustration of the frequency response of an accelerometer (left) and an acoustic emission sensor (right). The operating rage of the accelerometer is located to the left of the resonance peak where as the operating point of the AE sensor is near the peak of the response curve.

Both types of sensors are considered acousto-electric (AE) sensors because they convert mechanical vibrations into a corresponding electrical signal. Because the electrical noise environment of the HVT is so severe, the signal to noise ratio at the output of the AE sensor can be significantly reduced. Sensors and receiver equipment are shielded to lower their susceptibility to EMI, but are not completely immune. Despite this inherent noise problem, acoustic systems employing both types of sensors are used in commercial power plants. One system, the SPRTAN-AT, which employs 18 sensors[‡] affixed to the outside of a transformer tank, was able to produce a fault position to within an accuracy of 8 inches over the course of a 22 hour test while the transformer was operational [8]. Another reported system used 3 sensors[§] to determine a fault position bounded by a 200 mm cube over a 1-2 hour period, using multiple data captures while moving the sensors to gain better signal amplitudes [9]. The position accuracy of these systems fall within useful bounds, but the time it takes to find the position is much too long. Because a partial discharge can cause a failure in minutes or in hours, it is desirable for the results to be instantaneous or at least available in quasi-real time. One of the reasons that these calculations take so long is due to multipath interference. The sensors for the acoustic detection system are located outside the tank. The acoustic pulse can take several different paths along the transformer interior and exterior to reach the sensor. Therefore the same portion of the pulse can arrive at the same sensor at different times. This effect is exacerbated by the fact that the acoustic wave travels faster in the steel walls than in the fluid medium. While multipath effects can be removed, it requires multiple measurements of the PD as well as a large amount of computation time to accomplish. This speed limitation is one of the primary drawbacks of the external measurement systems. The multipath issue can be circumvented if the sensors are placed within the transformer tank. Internal systems have the advantage of measuring the acoustic wave directly from the liquid medium before reflection and multipath can distort the signal [10]. The problem with internal systems is that AE sensors cannot be placed within the transformer tank because they transmit an electrical signal that can interfere with the workings of the transformer. New acoustic sensor technologies that are suitable for the harsh environment of an HVT must be developed.

One such technology, fiber optic sensing, is making it possible for acoustic sensors to be placed inside the HVT. Fiber optic technology is ideal for this application because the devices are chemically and electrically inert. Therefore the sensor can be placed within the HVT tank

---

[‡] Sensors operated between the frequencies of 100 and 300 kHz with a resonance frequency of 150 kHz.
[§] Sensors operated between the frequencies of 50 and 200 kHz.

without damaging or even altering the operation of the transformer. Also, because the fiber sensor uses an optical signal to measure acoustic waves, the sensor is completely immune to EMI. There are several interferometry-based designs for fiber optic acoustic sensors [11] [12]. The following chapters describe the use of an extrinsic Fabry-Perot interferometric fiber optic sensor, developed at the Center for Photonics Technology at Virginia Tech, for PD detection and location.

Section 2.4: References

[1] S. A. Boggs, "Partial Discharge: Overview and Signal Generation," in *IEEE Electrical Insulation Magazine*, vol. 6, 1990, pp. 33-39.

[2] S. A. Boggs, "Partial Discharge - Part III: Cavity-Induced PD in Solid Dielectrics," in *IEEE Electrical Insulation Magazine*, vol. 6, 1990, pp. 11-20.

[3] I. J. Kemp, "Partial discharge plant-monitoring technology: Present and future developments," *IEE Proc.-Sci. Meas. Technology*, vol. 142, pp. 4-10, 1995.

[4] G. C. Stone, "Partial Discharge - Part VII: Practical Techniques for Measuring PD in Operating Equipment," in *IEEE Electrical Insulation Magazine*, vol. 7, 1991, pp. 9-19.

[5] M. Duval, "Dissolved Gas Analysis: It Can Save Your Transformer," in *IEEE Electrical Insulation Magazine*, vol. 5, 1989, pp. 22-27.

[6] L. E. Lundgaard, "Partial Discharge - Part XIII: Acoustic Partial Discharge Detection - Fundamental Considerations," in *IEEE Electrical Insulation Magazine*, vol. 8, 1992, pp. 25-31.

[7] L. E. Lundgaard, "Partial Discharge - Part XIV: Acoustic Partial Discharge Detection - Practical Application," in *IEEE Electrical Insulation Magazine*, vol. 8, 1992, pp. 34-43.

[8] P. M. Eleftherion, "Partial Discharge XXI: Acoustic Emission-Based PD Source Location in Transformers," in *IEEE Electrical Insulation Magazine*, vol. 11, 1995, pp. 22-26.

[9] V. Darley, "Partial Discharges within Power Transformers and the Use of Ultrasonic Techniques in Their Location," presented at IEE Colloquium on Assessment of Degradation Within Transformer Insulation Systems, London, U.K., 1991.

[10] B. T. P. a. R. E. J. T.R. Blackburn, "Optical Fibre Sensor for Partial Discharge Detection and Location in High-Voltage Power Transformer," presented at Sixth International Conference on Dielectric Materials, Measurements and Applications, Manchester, U.K., 1992.

[11] M. M. Zhao Zhiqiang, and M. Suleyman Demokan, "The Directionality of an Optical Fiber High-Frequency Acoustic Sensor for Partial Discharge Detection and Location," *Journal of Lightwave Technology*, vol. 18, pp. 795-806, 2000.

[12] H. X. Jiangdong Deng, Wei Huo, Ming Luo, Russ May, Anbo Wang, and Yilu Liu, "Optical fiber sensor-based detection of partial discharges in power transformers," *Optics and Laser Technology*, vol. 33, pp. 305-311, 2001.

Chapter 3: Sensor System Design

The two main objectives of this project are to detect partial discharges in HVT and to locate the source of that discharge using an optical acoustic sensor. The system used to meet the first objective by sensing and recording PD events is described in this chapter. The following chapter describes the signal processing required to locate the PD source.

The basic structure of any general PD detection system, not just optical acoustic systems, contains four parts: the sensor, the filter, the preamp, and the data acquisition system. The block diagram in Figure 3.1 illustrates the functionality of each component. Every PD detection system needs a device to detect the signal (the transducer), a device to separate the detected signal from noise (the filter), a device to increase the power of the signal (the preamp), and a device to record the captured signal (data acquisition). This chapter details the operation of the fiber optic sensor head and its connected instrumentation as they correspond to this basic four-block structure [1].

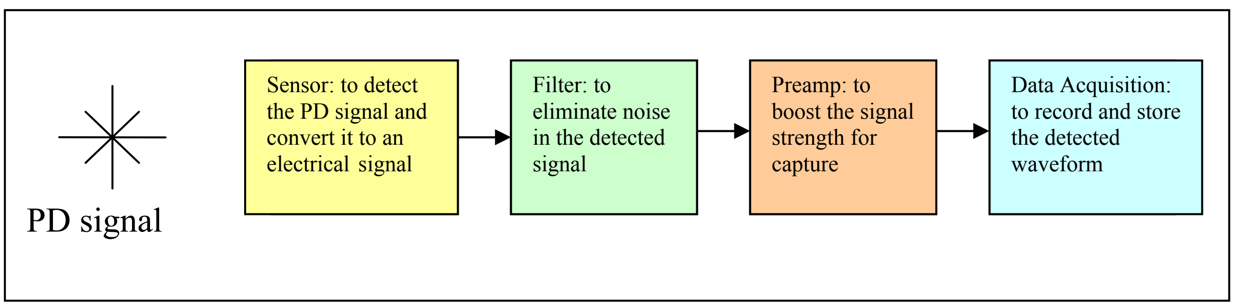

Figure 3.1: Block diagram of a generic PD detection system.

Section 3.1: Sensor Implementation in High Voltage Devices

Figure 3.2 illustrates how an optical acoustic (OA) PD sensor and its associated hardware could be implemented in HVTs. The sensor array is placed inside the tank so that the acoustic waves can be directly captured from the transformer oil, thus avoiding multipath problems. An optical fiber connects the internal sensor to the external optoelectronic signal processing unit. The sensor's interferometric signal is modulated by the incident acoustic wave, which can be recovered and converted into an electrical signal that is recorded using a digital oscilloscope. The OA sensor head functions as the transducer; filtering and pre-amplification are realized in the signal processing unit, and A/D conversion and data storage are performed by the digital oscilloscope.

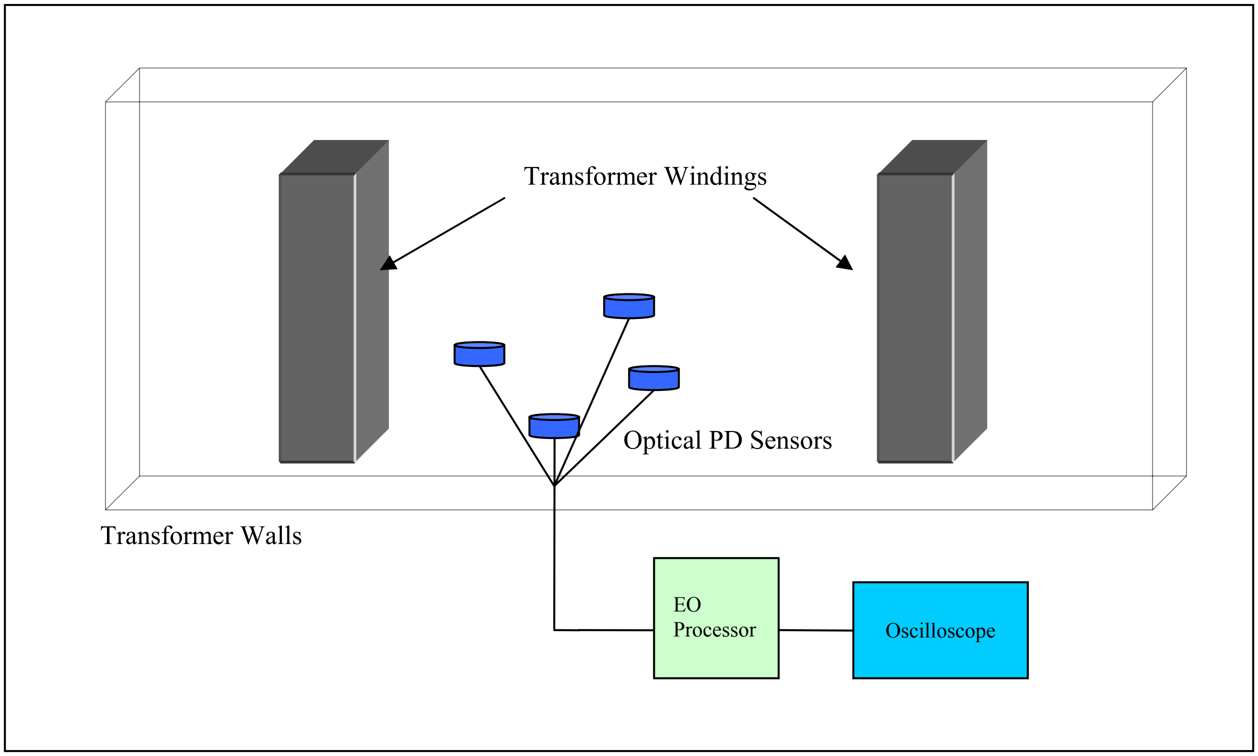

Figure 3.2: Illustration of how the internal optical acoustic PD detection system can be implemented in HVTs. The sensors are placed inside the tank while a fiber optic line connects the internal sensors to the external electro-optic processor. The optical signal from the sensor is demodulated and converted to an electrical signal by the EO processor. That electrical signal is then recorded using an A/D converter, which is implemented by using a digital oscilloscope.

Section 3.2: Sensor Operation

This project investigates the use of an OA sensor based on the extrinsic Fabry-Perot interferometer (EFPI). The sensor head, shown in detail in Figure 3.3, consists of an EFPI cavity formed by a single mode optical fiber secured in a silica tube and a deformable silica diaphragm.

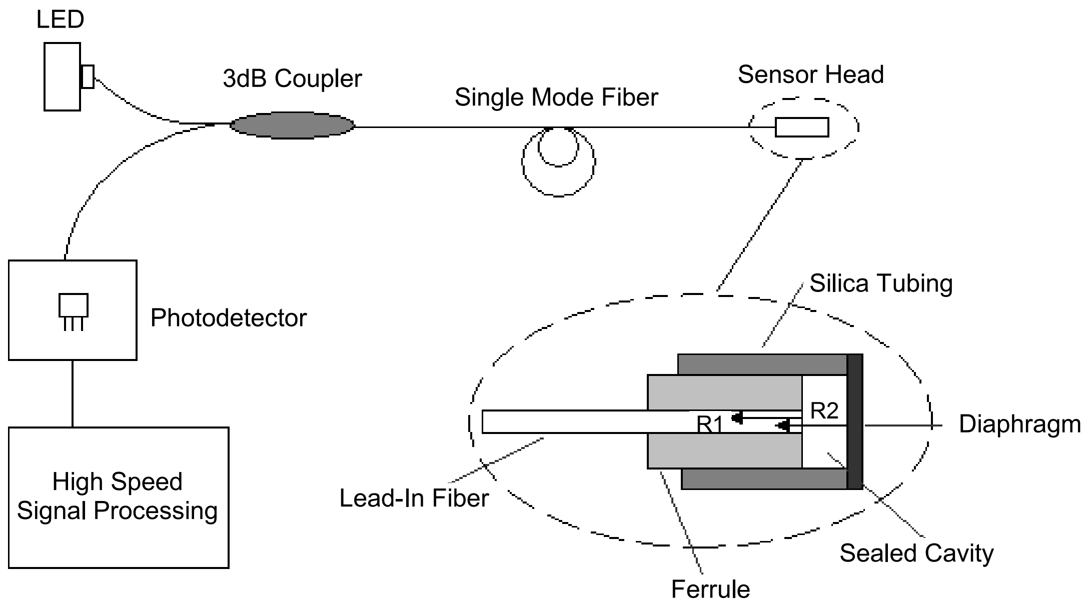

Figure 3.3: Detailed illustration of the EFPI based AO sensor. The exploded view shows the details of the sensor head.

The output from an LED with λ_0 = 1300 nm travels through a 2x2 coupler and down the fiber. The cleaved end of the fiber causes the first reflection of the interferometer. The remaining light is transmitted from end of the fiber and reflected off the silica disk, which is secured to the end of the tubing at a fixed distance from the end of the fiber. The ray that strikes the center of the diaphragm is coupled back into the fiber and interacts with the first reflection, producing an interference pattern. This optical signal travels back down the fiber to a photodetector where the intensity is measured. An incident acoustic wave will modulate the distance between the end of the fiber and the reflection point on the diaphragm by flexing the diaphragm, and therefore altering the interference fringe. The change in intensity varies linearly with small changes in gap distance when the sensor is operated over the linear range, as illustrated in Figure 3.4.

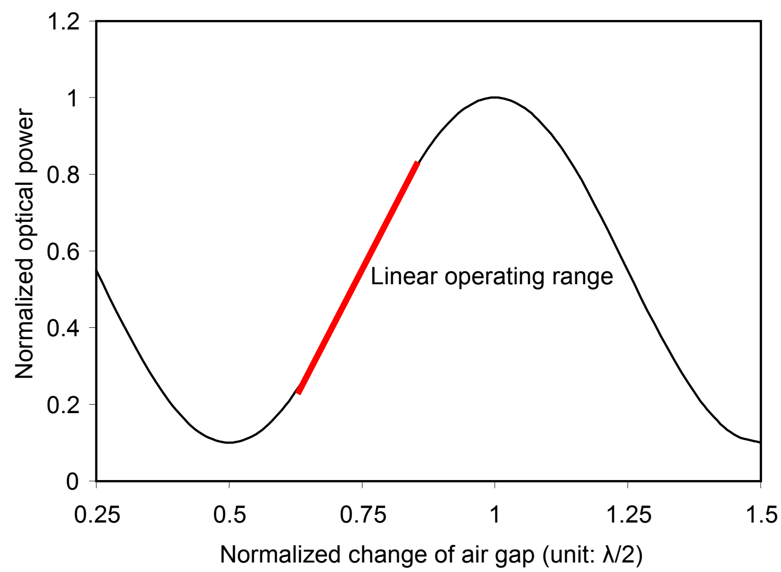

Figure 3.4: Variation of the output intensity as a function of the air gap distance.

The sensor is designed in such a way that when no acoustic signal is present, the intensity seen at the photodetector lies in the center of the linear region of the above operating curve, which is about 60% of the half period. As the length of the air gap changes, the intensity of the received signal will travel up and down this curve with respect to the center operating point. If the received signal falls outside of this linear 60% but is still within the half period, the demodulated signal will no longer vary linearly with the air gap change and will give an erroneous measure of the magnitude of the acoustic wave. If the signal falls outside of the half period an ambiguity problem results because the optical intensity correlates to more than one value for the air gap length. It is therefore extremely important that the sensor be designed in such a way that the incident acoustic wave will only cause linear changes in optical intensity. This determines the dynamic range of the sensor. For the 1300nm source used in this system, only deformations of ±200nm will be correctly decoded [2].

Section 3.3: Sensor Parameters

Section 3.3.1: Sensitivity

The magnitude of the diaphragm deformation is controlled by its sensitivity, which is defined as the amplitude of the diaphragm's deflection given a unit input of pressure. The center deflection of the diaphragm is given by [3]

$$y_0 = \frac{3(1-\mu^2)Pa^4}{16Eh^3} \qquad \textit{(Eq. 3.1)}$$

where y_0 is the maximum deflection, μ is the Poisson ratio, P is the applied pressure, a is radius of the diaphragm, E is the Young's Modulus for the material and h is the thickness of the diaphragm. For the diaphragm material utilized, E is fixed at 73.73 GPa because the diaphragm is made of silica and μ is 0.17 because only the first vibration mode of the diaphragm is being considered*. Therefore the acceptable pressure variation for this sensor is given by

$$P < 8227.096\frac{h^3}{a^4} \qquad \textit{(Eq. 3.2)}$$

and depends on the thickness and radius of the diaphragm. However, before the radius and the thickness can be chosen, the frequency response of the resulting sensor must be considered.

Section 3.3.2: Frequency Response

Another sensor parameter that is determined by the thickness and radius of the diaphragm is the frequency response. Diaphragms exhibit a characteristic frequency response that is flat for frequencies lower than its natural or resonance frequency. At the resonance frequency, the curve reaches a sharp peak and then decreases [3]. As mentioned in Chapter 2, the sensor can be operated as a broadband sensor, where the flat region of the frequency response covers the frequencies of interest or as a narrowband sensor where the center frequency of the signal is matched to the resonance frequency of the sensor. The resonance frequency of the diaphragm is described as [3]

* Only the first vibrating mode of the diaphragm is considered because the acoustic signal incident on the diaphragm in real systems will be too small to excite secondary modes.

$$f_n = \frac{\alpha h}{2\pi a^2}\sqrt{\frac{gE}{12w(1-\mu^2)}}$$ ***(Eq. 3.3)***

where h, a, E, and μ are as stated above, α is a constant defined by the vibration mode, g is the gravitational constant in m/s^2, and w is the specific weight of the material. For a broadband sensor, f_n is chosen to be much larger than the highest frequency of interest in the signal† while for a narrowband sensor, f_n is matched to the center frequency of the signal, f_c.

However, this equation for frequency response assumes that the diaphragm is not in contact with any viscous material on either side, and therefore cannot be used directly for PD detection within an HVT. In the case of the EFPI OA sensor, the diaphragm will be in contact with a very viscous liquid, mineral oil. Therefore, a correction term must be included in the resonance frequency calculation. The new resonance frequency becomes [3]

$$f_2 = \frac{f_n}{\sqrt{1+\beta}},\ \beta = 0.669\frac{w_1 a}{wh}$$ ***(Eq. 3.4)***

where f_n is the previously calculated resonance frequency, $w_1$is the specific weight of the viscous liquid and all other values remain as previously defined. This correction factor cannot be disregarded, as shown in Figure 3.5.

† For a broadband sensor, choosing f_n twice as large at the highest signal frequency is sufficient to guarantee a flat response over the region of interest.

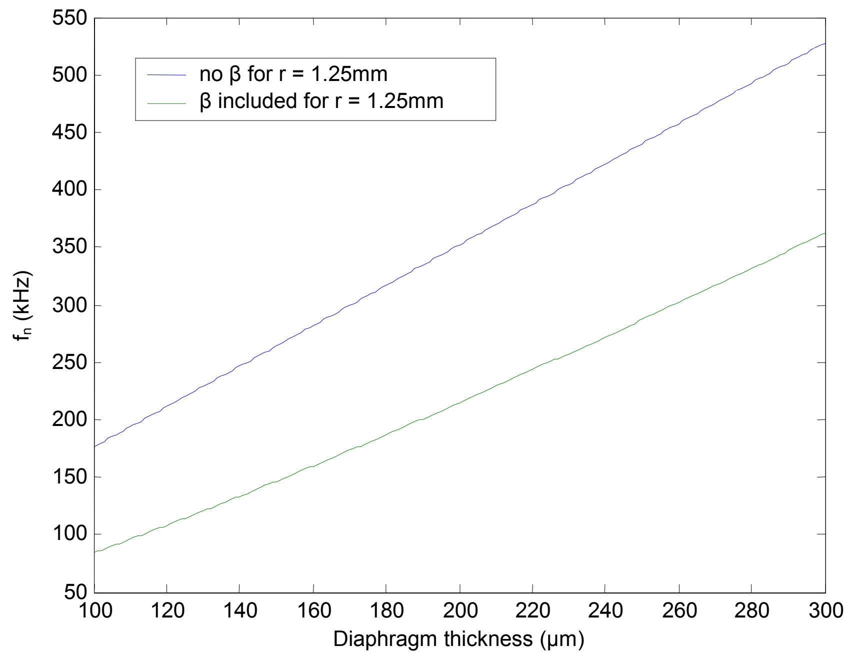

Figure 3.5: Plot of resonance frequency vs. the thickness of the diaphragm. For this analysis, MATLAB was used to evaluate the above equation and plot the results. The plot uses a fixed value for the diaphragm radius equal to 1.25mm.

The figure shows that as the thickness of the diaphragm increases, the correction factor β becomes increasingly important. This means that for higher frequency responses, the diaphragm used in the EFPI sensor used in a PD detection system will have to be much thicker than those used in open air applications.

But is there any disadvantage to having thicker diaphragms? The answer to that question is yes. Recall from Section 3.3.1 that the sensitivity of the diaphragm is defined as displacement per unit pressure. Using Eq. 3.1, the sensitivity is therefore inversely proportional to the cube of the thickness.

$$S = \frac{3(1-\mu^2)a^4}{16Eh^3}, \qquad \textbf{\textit{(Eq. 3.5)}}$$

If the thickness is increased, then the sensor's ability to distinguish between small variations in the pressure field created by the acoustic PD signal is reduced. Since PD signals are severely attenuated by the mineral oil, low sensitivity values could result in not detecting the PD event. On the other hand, if the thickness is decreased to increase sensitivity and the resonance frequency is too low, the signal may be corrupted by mechanical noise in the HVT or in the worst case not detected at all. Therefore, a trade off must be made: the thickness of the diaphragm should maximize sensitivity while meeting the frequency response requirements of the signal.

Unfortunately, there is very poor agreement in the literature as to the frequency content of an acoustic PD signal. Some sources recommend the use of a narrowband sensor with a center frequency of 150 kHz with a bandwidth covering 100-300 kHz [4] while others recommend a lower broadband frequency sensor covering the frequency range of 20-120 kHz [5]. The argument for using the higher frequency sensors is based on the fact that there is a significant acoustic noise source in the 50 – 60 kHz caused by the magnetostriction-induced core noise in the HVT, while the lower frequency sensor argument is based on the fact that the higher frequencies of the acoustic signal are attenuated severely by the transformer oil [5]. In the interest of limiting the external noise in the signal to obtain a higher initial signal to noise ratio (SNR), the higher frequency range was selected. To achieve a center frequency of 150 kHz, using Figure 3.5, the thickness of the diaphragm should be 165 um[‡].

Section 3.4: Sensor Testing

Once sensor parameters were set, the theoretical results were validated with experimental data. In order to verify that the frequency response of the 165µm EFPI OA sensor is centered around 150 kHz, a test rig was built in the CPT lab. It should be noted that the sensor testing was performed in water and not mineral oil. This substitution was made for two reasons. First, the acoustic attenuation in oil is so severe that the available acoustic PD simulator could not produce a high enough amplitude signal at sufficient distances. Second, water is readily available and could validate the theory of sensor design without adding lag time or cost.

Section 3.4.1: Test Methodology

The frequency response testing consisted of two parts. The first test was used to quantify the characteristics of the tank environment utilizing two piezoelectric transducers (PZTs) with

[‡] Using Figure 3.5 assumes that the radius of the diaphragm is 1.25mm. This assumption is made because the only silica tubing available at the Center for Photonics Technology (CPT) for sensor fabrication has an inner radius of 1.25mm. Therefore, all testable sensors have a diaphragm radius of 1.25mm.

known frequency responses as the source and acoustic receiver. The second part determined the response of the optical fiber sensor. Figure 3.6 is a block diagram of the experiment.

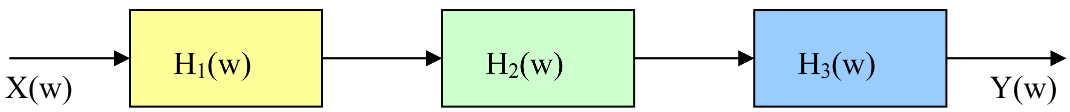

Figure 3.6: Block diaphragm that represents the variables in the lab experiment. X(w) is the frequency content of the electrical signal passed to the PZT source, H_1(w) is the frequency response of the PZT source, H_2(w) is the frequency response of the water, tank walls, etc., H_3(w) is the frequency response of the PZT or fiber sensor and Y(w) is the frequency content of the measured output signal.

In Figure 3.6, X(w) represents the Fourier transform of the input driver signal, H_1(w) is the frequency response of the PZT as a source, H_2(w) is the frequency response of the environment[§], H_3(w) is the frequency response of the PZT as a sensor, and Y(w) is the Fourier transform of the output signal captured by the scope. The signals X(w) and Y(w) are obtained by using the fast Fourier transform (FFT) function on an oscilloscope.

Since X, H_1, H_3, and Y are either known, measured, or derived quantities, H_2 can be found using the relation

$$H_2 = \frac{Y}{XH_1H_3} \quad . \qquad \textit{(Eq. 3.6)}$$

Once H_2 is calculated the second part of the experiment can take place. The system was setup again, replacing the PZT sensor with the fiber sensor. The same block diagram applies except that in this case H_3 is the unknown quantity. H_3 can then be calculated by

$$H_3 = \frac{Y}{XH_1H_2} \quad . \qquad \textit{(Eq. 3.7)}$$

However, this approach required that two sets of calculations be made. If only one calculation could be made based solely on measured or known quantities, then the calculated

[§] The environment consists of the tank, the water and any noise caused by the electric sources or measurement devices. Since all equipment is common to both tests, this technique allows all the noise sources to be removed from the measurement of H_3 for the fiber sensor.

frequency response would be more accurate because it was not based on a secondary calculation. Recall that

$$Y = X \times H_1 \times H_2 \times ... \times H_i \qquad \textbf{\textit{(Eq. 3.8)}}$$

where Y is the output of the system, X is the input and H_i is the impulse response of the ith component of the system. If this equation is converted into decibels** then the multiplicative relationship becomes additive and the above equation becomes

$$Y = X + H_1 + H_2 + ... + H_i \quad dB \qquad \textbf{\textit{(Eq. 3.9)}}$$

If the two impulse response tests are written in this mathematical form, then

$$Y_1 = X_2 + H_a + H_b + H_c \quad dB \qquad Y_2 = X_1 + H_a + H_b + H_d \quad dB \qquad \textbf{\textit{(Eq. 3.10)}}$$

where Y_2 and Y_1 are the measured output from each test, X_1 and X_2 are the identical inputs to the system, H_a is the impulse response of the transmitter used in both tests, H_b is the impulse response of the environment, H_c is the impulse response of the receiving PZT and H_d is the impulse response of the fiber sensor. If the above equations are subtracted, the following relationship results:

$$H_d = Y_2 - Y_1 + H_c \qquad \textbf{\textit{(Eq. 3.11)}}$$

Therefore, neither the impulse response of the environment nor the transmitter nor the frequency content of the input is needed to determine the unknown impulse response of the fiber sensor. This reduced form decreases the amount of information needed for the fiber sensor impulse response calculation as well as eliminates the need for the intermediate environmental impulse response calculation.

Section 3.4.2: Test Set Up

Both parts of the frequency response test took place in the same physical environment. Figure 3.7 illustrates the test setup. The testing occurred in a 10-gallon glass tank filled with

** Decibel conversion in this document refers to dB(.) = 10*log (.).

water and the source and sensors were mounted inside of 1 ¼ inch diameter PVC tubing. The mounting process involved drilling a hole in the tube, which had been cut to a 12-inch length to fit in the tank, and securing the sensors using LEXEL, a rubber based glue. PVC pipe was used because it is round, which allowed for no direct reflection into the transmit or receive path, and it is easy to manipulate. The flexible adhesive was used in lieu of epoxy so that the sensors could be recovered and reused in future experiments. The two pipes were fitted together with a long ¼ inch threaded rod and secured into place with hex nuts. Using a threaded rod allows for different measurable distances to be established between the source and the sensor. Figure 3.8 is a picture of the actual test rig in the lab.

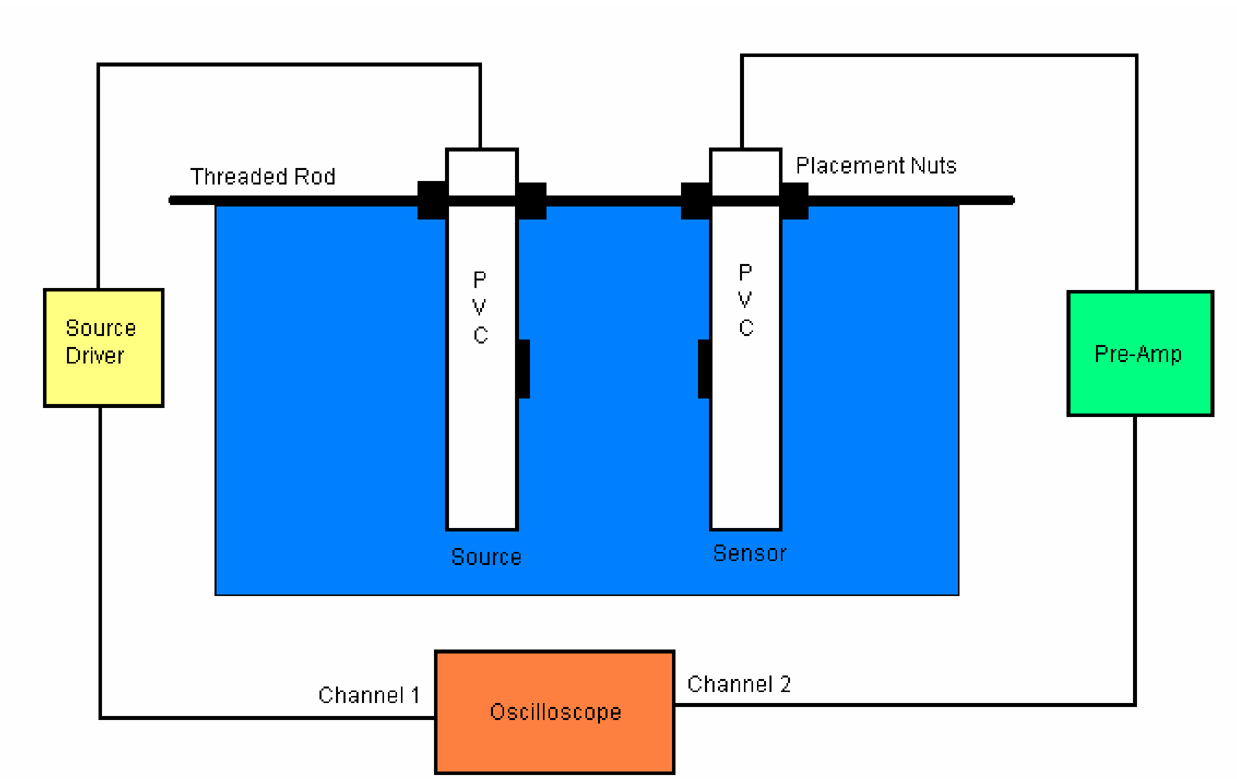

Figure 3.7: Illustration of the test setup and associated recording and source equipment.

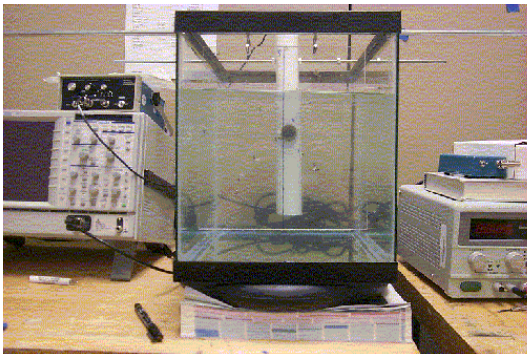

(a)

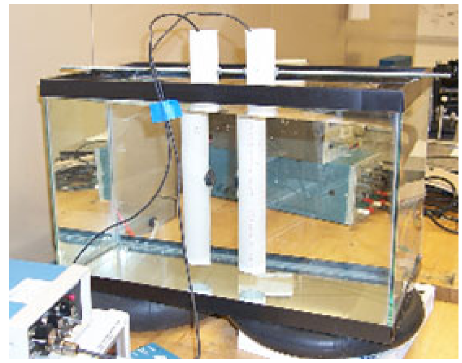

(b)

Figure 3.8: Pictures of the test rig from the front (a) with more detail on the tank geometry (b).

The transmitting PZT was driven by a 40 μs pulse at a repetition rate of 23 kHz using a Physical Acoustics C-101-HV Pulse System Calibrator. All signals were monitored using a LeCroy Waverunner LT322 two channel oscilloscope with an external trigger connected to the source driver. The time domain data from the tests was converted to frequency domain data using a 200 point FFT algorithm on-board the scope and then exported in a comma delimited form through the floppy drive.

One potential problem with this set up is that the frequency response found for the experiment environment could depend on the distance between the sensor and the source. This could occur if the distance between the source and the surrounding walls was not adequate to keep multipath signals from interfering with the direct signal [6]. Using the knowledge of the speed of sound in water and the maximum pulse width of the PZT driver system, the minimum reflection path length can be calculated. For the forward path (transmitter to opposite wall and back) the reflection path must follow

$$d_1 + d_2 + d_1 > pulsewidth_{\max} v \qquad \textbf{\textit{(Eq. 3.12)}}$$

where d_1 and d_2 are the distances between the tank wall and the source, and the source and sensor, respectively and v is the speed of sound in the water. The maximum pulse width is 40μs and v is 1480m/s, so the total length of the tank must be more than 6cm. The tank dimensions are longer than 6 cm in any direction, so multipath interference was not expected to be an issue.

Section 3.4.3: Test Results

<u>PZT to PZT Measurement</u>

Using the test rig illustrated above with the PZT reference sensor, the input and output spectra of the system were measured using an oscilloscope. Initial measurements were taken at separation distances of 4cm, 7cm, and 20cm. The input signal was measured from the echo port of the driver system and is shown in Figure 3.9, which illustrates its relatively broadband nature, as expected with a short pulse. However, in order to use the input test data for the frequency response calculation the stability of the source needed to be demonstrated. To test for stability, 15 measurements at 5 different distances over 2 days were taken and plotted on the same graph (Figure 3.10). It is evident that the signal was very stable as both a function of time and PZT separation. Therefore an average of the input signal can be used to represent X(w) in all calculations.

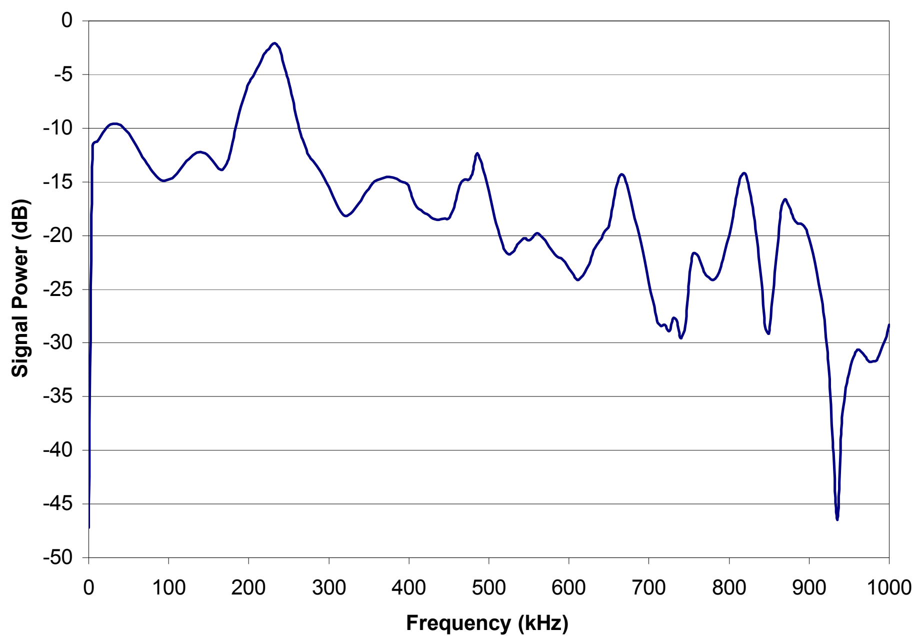

Figure 3.9: Plot of the spectrum of the input signal created by the Physical Acoustics driver. The plot was created by averaging the three data sets taken when the two PZTs were separated by 4cm, 7cm, and 12cm.

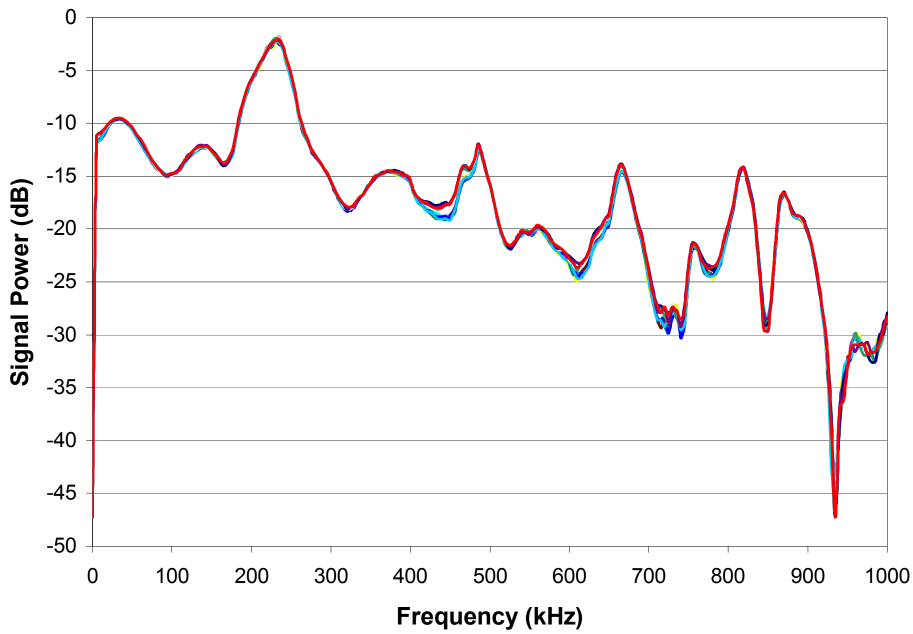

Figure 3.10: Plot of the spectrum of 15 different samples of the input signal at separations of 4, 7, 12, 16 and 20cm.

The measurement of the output signal was obtained using the same equipment. However, the output was measured from the output port of the Physical Acoustics 1220A Preamplifier. The amplifier has a flat frequency response over the frequency band of interest and increases the signal from the PZT receiver by a factor of 40dB. Therefore, 40dB was subtracted from the data used to generate the plots shown below. Figure 3.11 is a plot of the average output at 4cm, 7cm and 20cm[††].

[††] Justification for the use of the average output is the same as for the input. The samples for each distance were plotted individually and judged stationary by inspection in each case.

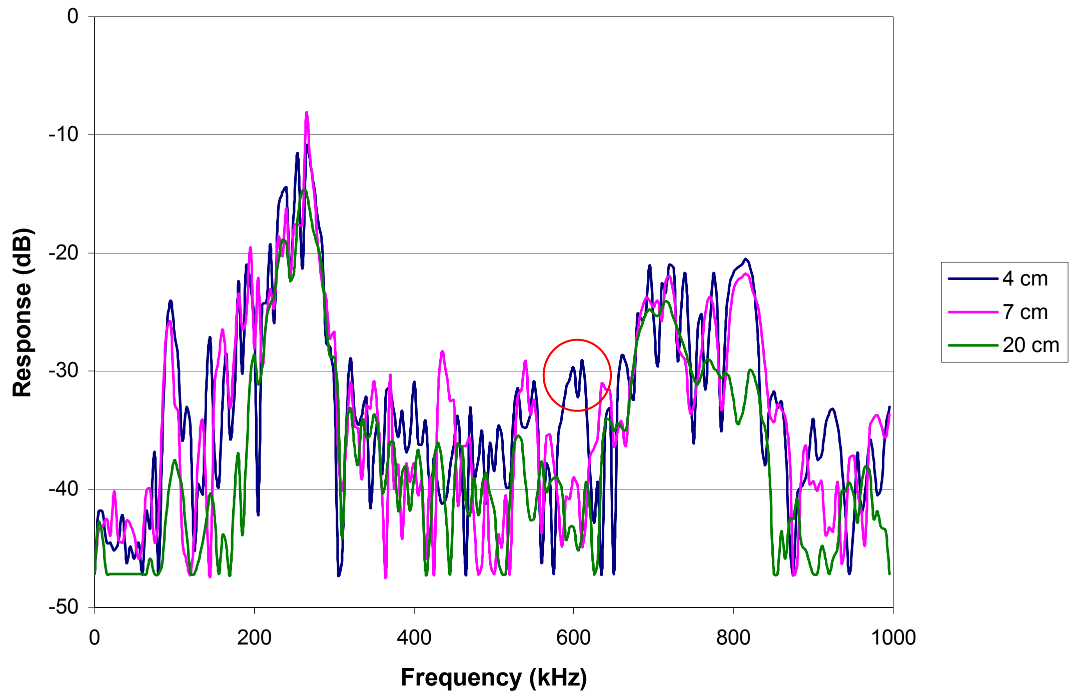

Figure 3.11: Plot of the average output of the PZT sensor at 4cm, 7cm, and 20cm. The red circle highlights an anomalous region in the data.

With the exception of one area, the data collected at these three points follows the expected trend; that is, as the range increases, the magnitude of the received signal decreases due to spherical wave spreading and attenuation by the water in the tank. However, there is one anomalous region centered on 600 kHz. At 4cm, the received signal is 10dB higher than at 7cm but the difference between 7cm and 20cm is only 5dB.

The experiment was repeated at 4cm to confirm the existence of a peak in that frequency range. Then the separation distance was increase in smaller increments to determine if the phenomenon was due to nonlinear absorption or some other factor. Figure 3.12 is a plot of average outputs from 4cm to 12cm in steps of 1cm as well as two measurements taken at 16cm and 20cm.

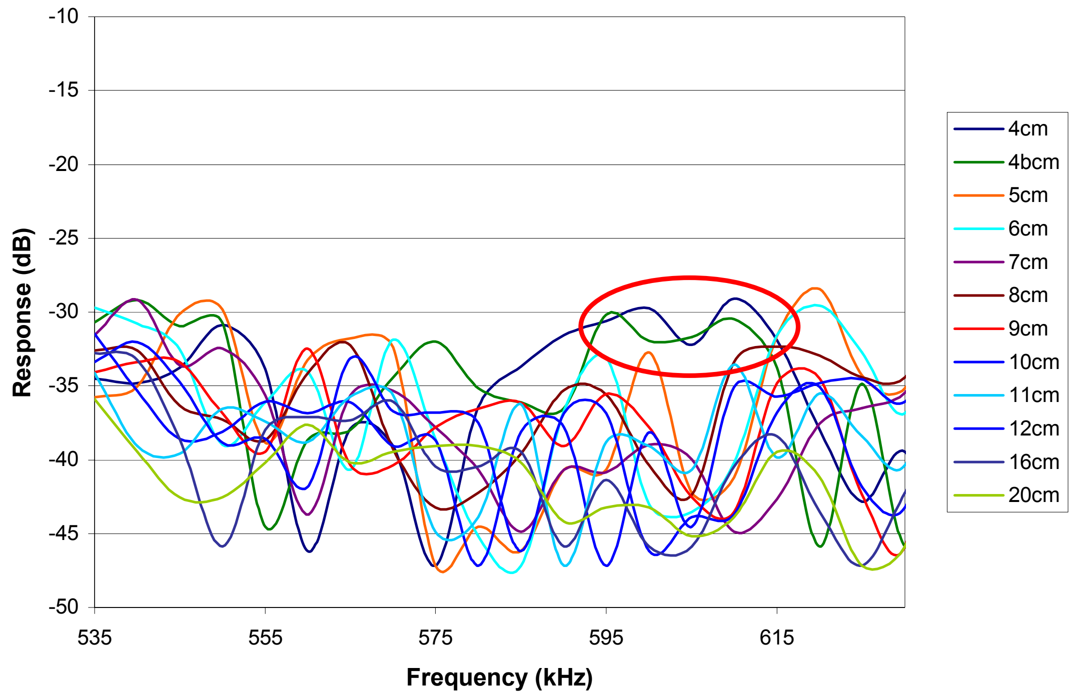

Figure 3.12: Plot of received signal spectrum from PZT sensor at varying distances. The red circle on the graph highlights the position of the peak witnessed at 4cm. Note that the pink line labeled 4bcm represents the second data collect at 4cm.

The close proximity of the two 4cm data sets Figure 3.12 confirms the existence of a peak around 600 kHz. However, at distances greater than 4cm, the peak is distinctly absent. Therefore, it must be concluded that the peak is caused either by reflection between the sensors, which is then amplified by the fact that the impulse response of the sensor has a resonance around 600 kHz, or by some near field phenomenon caused by the receiver being too close to the acoustic source. To eliminate the possibility of measuring near field anomalies, measurements using the fiber sensor were not performed at separations less than 6cm.

The data shown in Figure 3.10 and Figure 3.12 provide the input, X(w), and the output, Y_1(w), of experiment consisting of the two PZTs. The only remaining piece of data relating to the PZT measurement was the impulse response of the PZT receiver, which was obtained from the manufacturer. The PZT receiver was then replaced with a fiber sensor and the experiment repeated to obtain Y_2(w).

Fiber Sensor Measurements

The frequency response testing of a 150μm EFPI OA sensor was performed using the same test set up illustrated in Figure 3.7. To ensure that the results of the testing truly verified the theory presented in Section 3.3.2, two sensors were tested. The output of each sensor was recorded 10 times at 5 different distances to ensure that the results were stationary as a function of time and decreased linearly as a function of distance. Ten data sets were obtained by using the FFT function[‡‡] of the oscilloscope at each of the distances, 7, 8, 9, 10 and 12 cm. For each of the 10 trials, 500 data points were taken between zero and 500 kHz. The data was then imported into an Excel spreadsheet for analysis. Representative data collected at 7cm is shown in Figure 3.13.

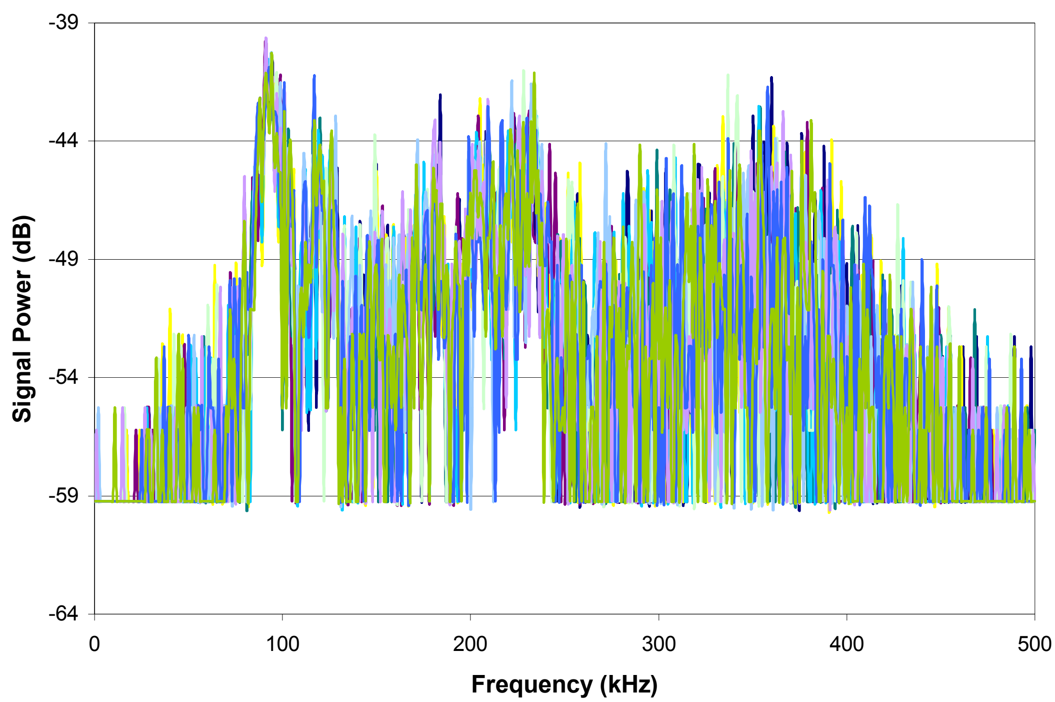

Figure 3.13: Frequency content of 10 samples taken by a 150μm sensor placed 7 cm from the source.

[‡‡] The FFT for each of the time signals was obtained while the scope was set at a time resolution of 0.1ms per division and a voltage resolution of 0.5 V per division. These settings were fixed during the data collection process for both the PZT to PZT test as well as the fiber sensor test because the magnitude of the FFT depended linearly on these settings. The bias created by these settings subtracts out in the frequency response calculation and are therefore of no consequence to the final result.

The plot shows that, unlike the PZT-to-PZT experiment, the data was not stationary between each of the time samples. Since the source was demonstrated to be stationary with respect to time, it is evident that the noise from the electro-optical receiver was not stationary in time and was much greater than the noise present in the PZT receiver system. The signals were therefore filtered by a two, three and four point simple moving average, shown in Figure 3.14 for a 150 μm sensor[§§]. Although the EO receiver contains an electrical low pass filter with a cut off of 300 kHz, Figure 3.14 shows the data collected out to 350 kHz in order to illustrate the 3dB signal to noise improvement achieved using a four point moving average, which was used for the remainder of the experiments.

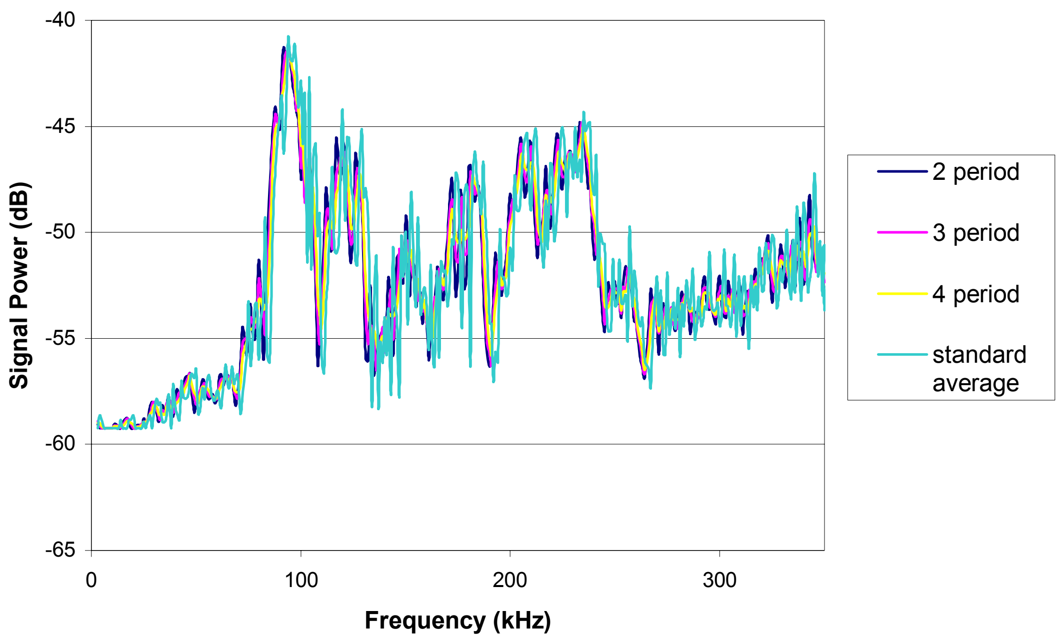

Figure 3.14: 10 set standard average and the two, three, and four period moving average of the standard average. All computations are based on data taken when the fiber sensor was 7 cm from the PZT source.

Once the output, $Y_2(w)$, of each of the two sensors was calculated, the frequency response of each of the sensors was determined using the data from the fiber sensor experiment

[§§] 150 μm refers to the thickness of the diaphragm used in the sensor to modulate the air gap between the end of the fiber and the end of the sensor.

and the PZT to PZT experiment, and the known frequency response of the PZT receiver. Figure 3.15 shows a plot of the first sensor's frequency response at each of the five distances. While there is still a significant amount of noise in the calculated responses, a 6th order polynomial fit (Figure 3.16) can be used to illustrate the general trends. The frequency response of the 150 um sensor is suppressed at 50 kHz and has a relatively flat region between 100 kHz and 250 kHz. This result is promising for a number of reasons. First, it validates the diaphragm theory presented in Section 3.3.2; second, the mechanical core noise between 50 and 60 kHz present in a transformer will be suppressed by this sensor; and third, the PD signal to be captured has significant frequency content between 100 and 300kHz. This means that there will be little distortion of the signal by the sensor.

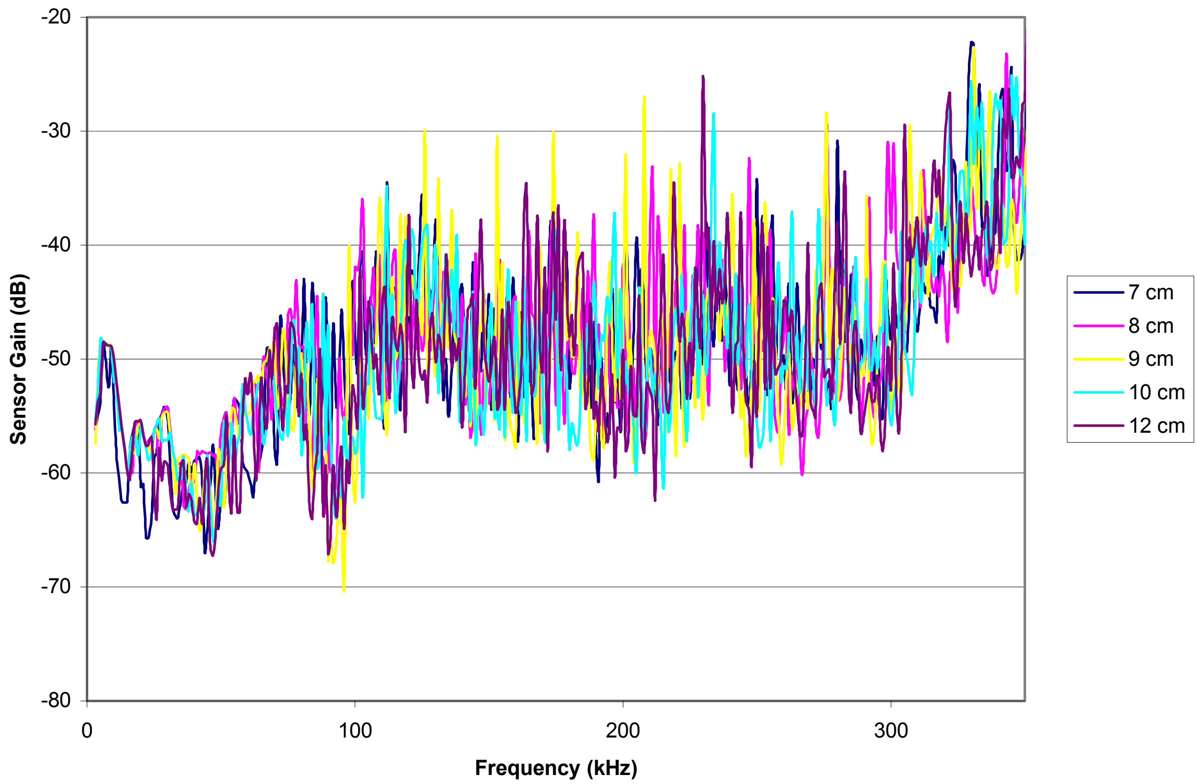

Figure 3.15: Results of the frequency response testing of sensor 1. Each line represents the frequency response calculated using data from the five distances, which was averaged using a standard average and then averaged again using a 4 period moving average to lower the effect of noise. The calculation was performed in MS Excel and followed Eq. 3.11.

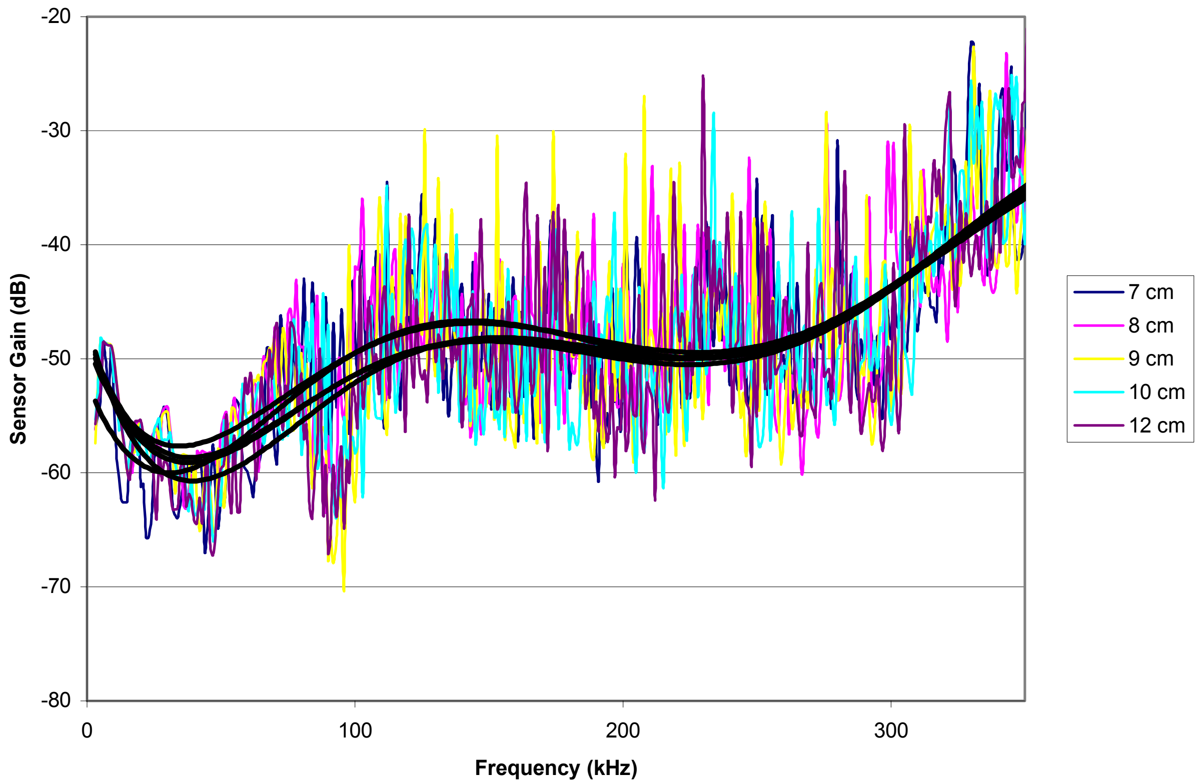

Figure 3.16: Plot of the calculated frequency response for sensor 1 with the associated 6th order polynomial fit lines.

The calculated frequency response of the second sensor, also a 150µm sensor, is shown in Figure 3.17.

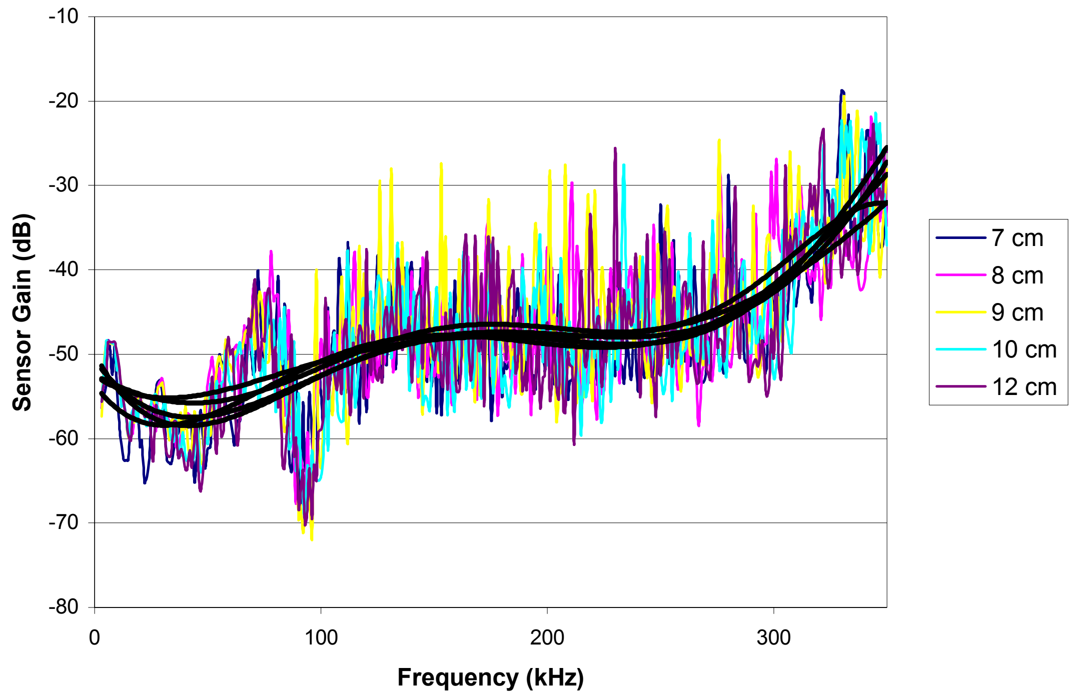

Figure 3.17: Results of the frequency response testing for sensor 2. Plot shows the frequency response calculated at the five distances and the associated 6th order polynomial fit line for each distance. Frequency response data was processed in the same manner as the data for sensor 1.

Comparing Figure 3.16 and Figure 3.17, the same general shape can be extrapolated from both sets of collected data. However, there is a difference in the value of the null around 50 kHz, which is less pronounced in the second sensor, and the flat response region seems to be shifted by 25 kHz though the bandwidth remains the same. This shift is probably caused by the fact that the manufacturing process for the sensor is not automated. Slight deviations in the effective radius of the diaphragm can occur if the bonding material spreads beyond the edges of the silica tubing. Therefore, the frequency response is expected to differ slightly between sensors. It is also noticeable in Figure 3.17 that the trend lines are not as closely clustered as the lines created for the first sensor. This deviation is most likely attributable to the fact that the signal to noise ratio for the second sensor was lower than that of the first 150 μm sensor and so the transient noise had a greater effect on the data collected using the second sensor. However, these lines are sufficiently close to discern a shape for the frequency response of the second sensor.

The results of these tests demonstrate that the 150μm EFPI OA sensor is capable of detecting an acoustic signal from the simulated PD source. In addition, this particular sensor is capable of providing reliable pulse characteristics because the frequency response of the sensor is flat over the PD signal frequencies and the pulse experiences little distortion. The next step in the research was to determine and test a methodology for locating a PD source in an HVT tank.

Section 3.5: References

[1] A. Z. a. T. R. Blackburn, "Acoustic Detection of Partial Discharges Using Non-Intrusive Optical Fibre Sensors," presented at IEEE International Conference on Condution and Breakdown in Solid Dielectrics, Vasteras, Sweden, 1998.

[2] H. X. Jiangdong Deng, Wei Huo, Ming Luo, Russ May, Anbo Wang, and Yilu Liu, "Optical fiber sensor-based detection of partial discharges in power transformers," *Optics and Laser Technology*, vol. 33, pp. 305-311, 2001.

[3] M. Di Giovanni, *Flat and corrugated diaphragm design handbook*, vol. 11. New York: M. Dekker, 1982.

[4] P. M. Eleftherion, "Partial Discharge XXI: Acoustic Emission-Based PD Source Location in Transformers," in *IEEE Electrical Insulation Magazine*, vol. 11, 1995, pp. 22-26.

[5] B. J. Tord Bengtsson, "Transformer PD Diagnosis using Acoustic Emission Technique," presented at 10th International Symposium on High Voltage Engineering, Montreal, Canada, 1997.

[6] M. M. Zhao Zhiqiang, and M. Suleyman Demokan, "The Directionality of an Optical Fiber High-Frequency Acoustic Sensor for Partial Discharge Detection and Location," *Journal of Lightwave Technology*, vol. 18, pp. 795-806, 2000.

Chapter 4: Positioning System Design

The second objective of this project was to determine the position of the PD event based on signals from a sensor array within the transformer tank. Four tasks were required to implement the positioning system: 1) define the system parameters, namely the position accuracy; 2) select a positioning algorithm that is capable of providing the specified accuracy and implement that algorithm using a computer program; 3) simulate signals and test the algorithm's ability to meet the specifications; 4) test the system's performance using experimental data from the sensor.

Section 4.1: System Specifications

The purpose of locating a PD source is to identify and repair sites of insulation breakdown. Therefore, it is important to design for a position accuracy that is useful to plant monitoring personnel. In Chapter 3, two examples of positioning systems were given, one with 8-inch position accuracy [1] and another with an accuracy bounded by a 200mm cube[*] [2]. In other PD experiments, void PD simulation sources are typically between 1 - 10mm [3] and 1.5 – 2.5 cm [4]. Based on this information, a position accuracy of ± 5 cm on any axis was selected for this acoustic PD detection system.

A second parameter requiring definition is the time required to achieve a position lock with the defined accuracy. For a real time or quasi-real time system, the position determination must be made within one or two measurements of the PD event because the repetition rate of the PD signal may be on the order of minutes or hours. Therefore, the designed system must calculate a position within the set error bounds in one reading of the PD event in order to meet the requirement of real time positioning.

Section 4.2: Positioning Algorithm

The positioning algorithm employed to find the acoustic signal in a transformer tank is based on the range equations from a known point to the position of the source. Figure 4.1

[*] 200mm cube converts to a ±10cm deviation on the x, y, or z axis.

illustrates the geometry used to create the range equation in two dimensions. The range between the source and the sensor can be expressed in terms of the sides of a right triangle using the Pythagorean Theorem. Extending this geometry to three dimensions, the range is defined by

$$r_1^{\,2} = (x - x_1)^2 + (y - y_1)^2 + (z - z_1)^2 \qquad \textbf{\textit{Eq. (4.1)}}$$

where (x,y,z) are the coordinates of the source and (x_1,y_1,z_1) are the coordinates of the sensor. For each sensor in an array, one of these spherical equations can be written and a system of nonlinear equations is created. Many methods have been developed to solve systems of nonlinear equations. A common example is the Newton-Raphson method, which uses a Taylor Series expansion to linearize the set of equations and an iterative algorithm to find the solution given an initial guess. However, this method requires that the guess be close to the true position of the source and can be computationally expensive.

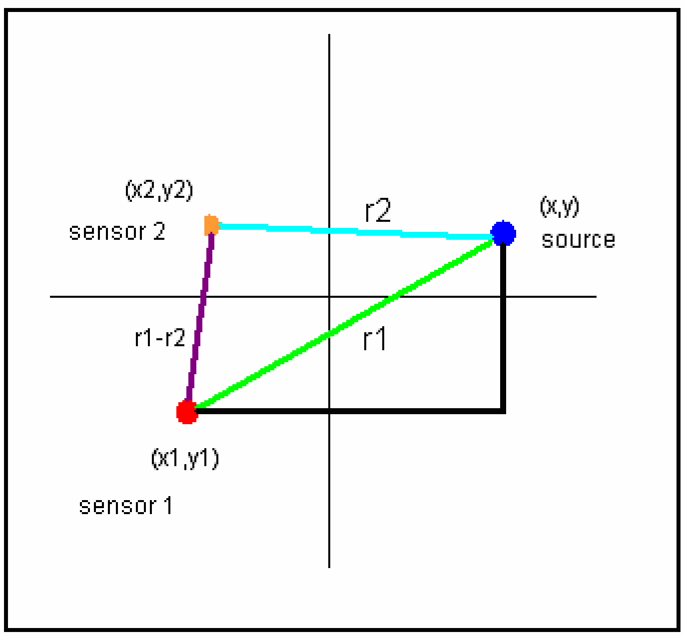

Figure 4.1: Geometry that defines the range equation between sensors and a source in the x-y plane.

An alternative to the Newton-Raphson Method is to form a difference equation using the range equations from two sensors. If the range is written as the speed of sound in the medium times the signal propagation time, then the difference equation can be written in terms of a time difference between two sensors. This leads to a system of linear equations[†] that relates the source coordinates to the unknown range from the first sensor to the source,

$$\begin{bmatrix} x \\ y \\ z \end{bmatrix} = -\begin{bmatrix} x_{21} & y_{21} & z_{21} \\ x_{31} & y_{31} & z_{31} \\ x_{41} & y_{41} & z_{41} \end{bmatrix}^{-1} \times \left\{ \begin{bmatrix} r_{21} \\ r_{31} \\ r_{41} \end{bmatrix} r_1 + \frac{1}{2} \begin{bmatrix} r_{21}{}^2 - K_2 + K_1 \\ r_{31}{}^2 - K_3 + K_1 \\ r_{41}{}^2 - K_4 + K_1 \end{bmatrix} \right\} \qquad \text{Eq.(4.2)}$$

where (x_{i1},y_{i1},z_{i1}) is the difference between the coordinates of the *i*th sensor and the first sensor, r_{i1} is the speed of sound in the medium times the time difference found between the first and the ith sensor, r_1 is the range from sensor 1 to the source, and $K_i = x_i^2 + y_i^2 + z_i^2$. If each of the source coordinates (x,y,z) are solved in terms of r_1, the resulting expressions can be inserted in the range equation for sensor 1 (Eq. (4.1)) in order to solve for r_1. Once the positive root of the quadratic equation is determined, the value of r_1 can be used in Eq. (4.2) to determine the source coordinates [5].

To understand how error in the TDOA calculation could impact the accuracy of this positioning system, the relationship between position error and TDOA error can be calculated assuming that the sensor positions are known to within ±0.5mm. Figure 4.2 shows the results of the calculation. For the error bound set in Section 4.1, the time difference must be known to within 4.6μs.

[†] The system contains three equations when four sensors are used.

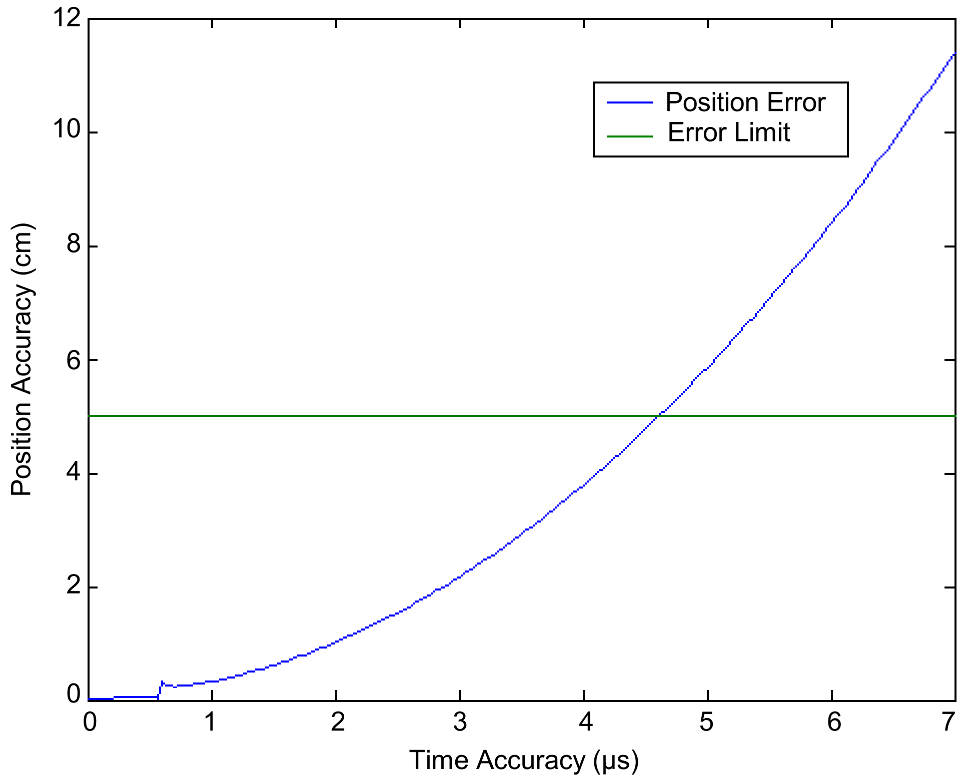

Figure 4.2: Error in position as a function of the TDOA accuracy. This plot was obtained by replacing all of the measured values in Eq. (4.2) with their uncertainty values. The uncertainty of the TDOA was varied between zero and seven microseconds and it was found that to obtain the ±5cm error bound in position, the TDOA for each sensor must be known to within 4.6μs.

Section 4.3: Time Difference of Arrival

The positioning algorithm that is presented here is an exact solution to the difference range equations if the acoustic velocity of the pulse is assumed to be constant and known. Therefore, the accuracy of the calculated position is determined by the uncertainty of the time difference of arrival found for each pair of sensors and the accuracy of the known sensor positions.

Section 4.3.1: High Pass Filtering

Edge detection using high pass filtering was initially evaluated for determining the time difference of arrival for each pair of sensors. Since the edge detail of a signal is contained in its high frequency components, a high pass filter can be employed to find the rising edge of each acoustic pulse. The time difference can then be calculated by subtracting the time locations of the each of the rising edges. To test this methodology, two gated sinusoids with a time delay were created in MATLAB. Figure 4.3 and Figure 4.4 show the two time domain signals and their Fourier transforms, which were obtained using the fast Fourier transform (fft). Each of the signals was filtered using an ideal high pass filter with a cut off frequency of 625Hz. The resulting time domain signals were then recovered using the inverse fast Fourier transform (ifft). Figure 4.5 shows the filtered time domain signals as well as the original signals. The rising edge of each of the gated sinusoids is marked by a sinc function. The time locations of the sinc function peaks were found using the max() function in MATLAB and subtracted to obtain the time difference between the two signals. Using this methodology, a time difference of 10.00μs is obtained, which is accurate to 0.01 μs.

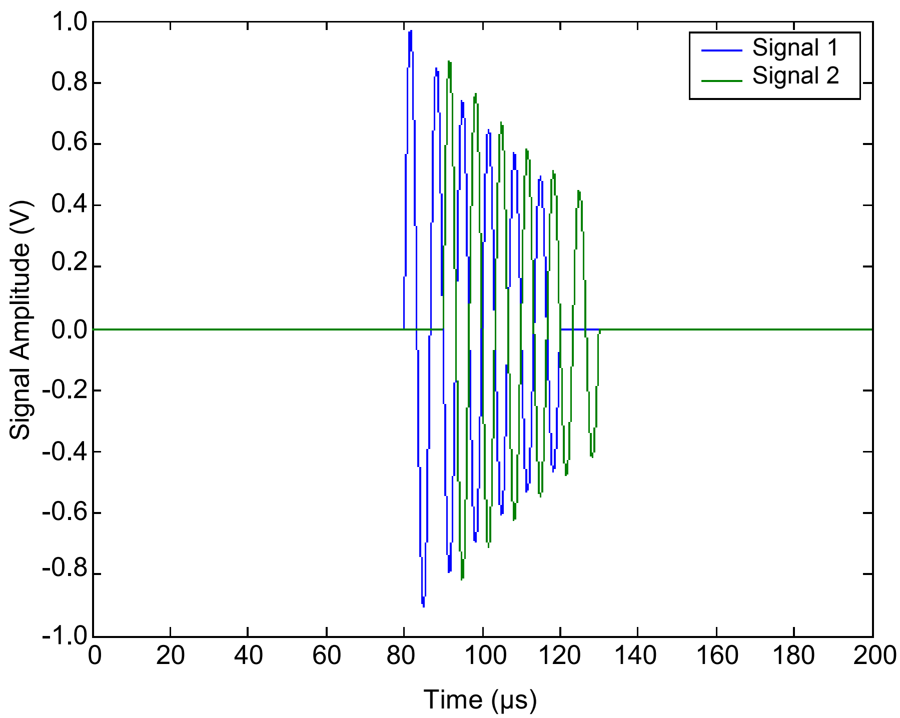

Figure 4.3: Plot of two simulated (noiseless) PD signals, gated sinusoids with a frequency of 150 kHz and a time separation of 10 μs. No noise has been added at this point in order to evaluate the accuracy of the filtering process itself.

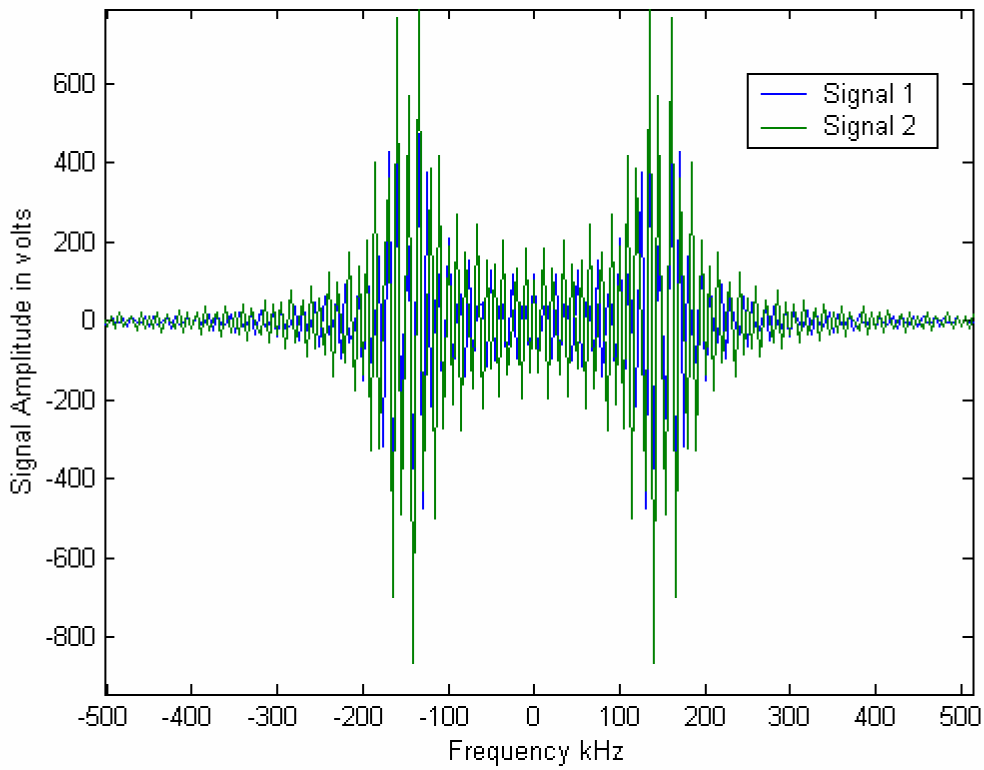

Figure 4.4: Fourier transform of the two gated sinusoidal signals in Figure 4.3, created using the fast Fourier transform (fft) function in MATLAB. The functions shown here are the pure sinusoidal signals with no noise added.

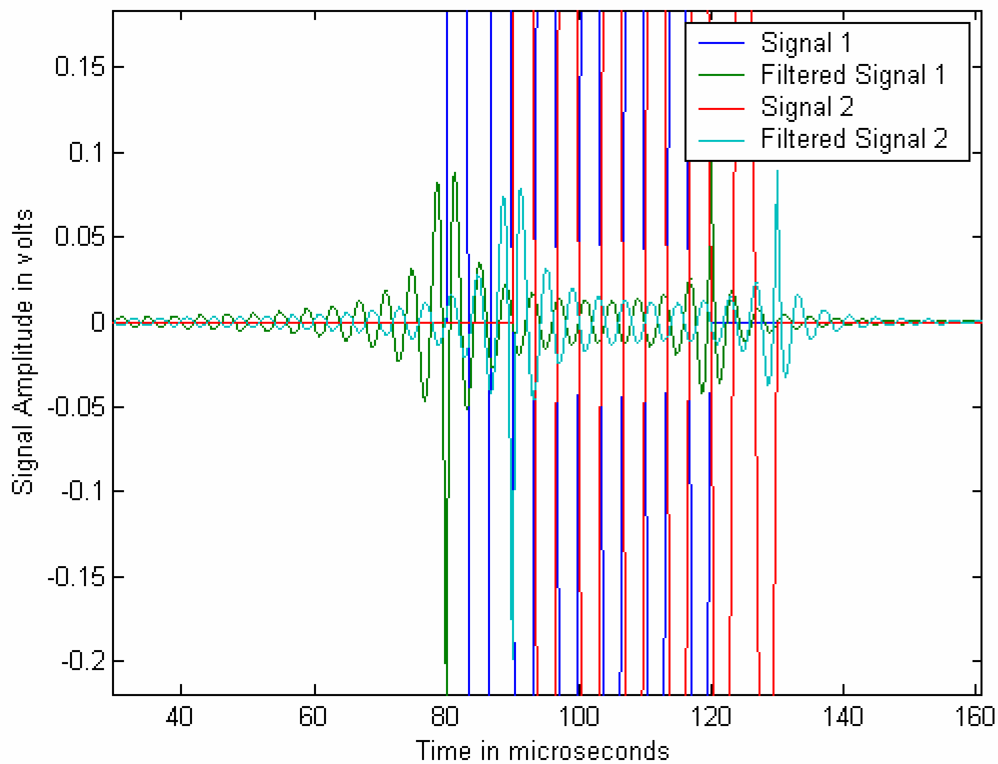

Figure 4.5: Comparison of original and filtered time domain signals using a high pass filter with a cutoff frequency of 625Hz. Note that for each of the gated sinusoids, a sinc-like function is created at the location of the rising edge of each signal. The time location of each of these peaks, when subtracted, yields the time difference between the two signals.

The filtering approach works well in the absence of noise. To evaluate its effectiveness for noisy signals, the random number generator in MATLAB was used to incorporate additive white noise into the two signals in Figure 4.3 for a SNR of 8dB (based on peak to peak values). Figure 4.6 shows the two noisy time domain signals and the result of the filtering process. The time delay between the two signals was found to be 4.987μs instead of 10μs, which would result in a location error of ±6cm. Therefore, alternatives to the filtering method were investigated for TDOA determination.

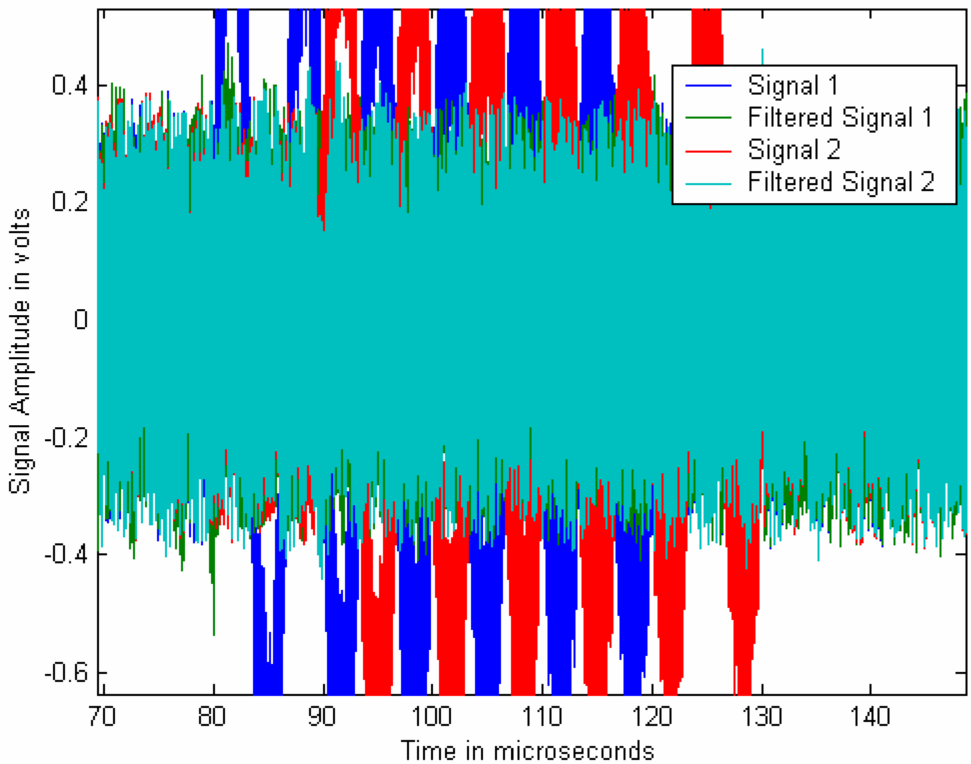

Figure 4.6: Simulated signals with additive white noise and the resulting filtered signals. The filter bandwidth is the same as that shown in Figure 4.5. The signal to noise ratio (SNR) for each signal is 8dB based on peak-to-peak values.

Section 4.3.2: Correlation

An alternate way to find the time difference of arrival between two sensor signals is to convolve the signals. Since the received signal is the same at both sensors, except for the time delay and intensity, the convolution becomes an autocorrelation‡ with a time shift. The time delay can be determined by locating the autocorrelation curve peak. If the signals were identical, the peak would be at zero, but the time shift causes the autocorrelation peak to shift by the same amount as the time delay. This was demonstrated using the correlation of two square wave pulses, resulting in the correct time delay, even in the presence of noise (see Appendix A). However, the signal received by the optical sensors is a gated sinusoid with very few periods within the envelope, as shown in the simulation in Section 4.3.1. Figure 4.7 shows the

‡ The convolution and correlation of two signals is the same if both signals are real. Only real signals were analyzed in this simulation because the signals captured in the operational environment will be purely real.

convolution of the two signals shown in Figure 4.3. Using the max() function again in MATLAB, the separation was found to be 9.98µs, an error of only 0.2%.

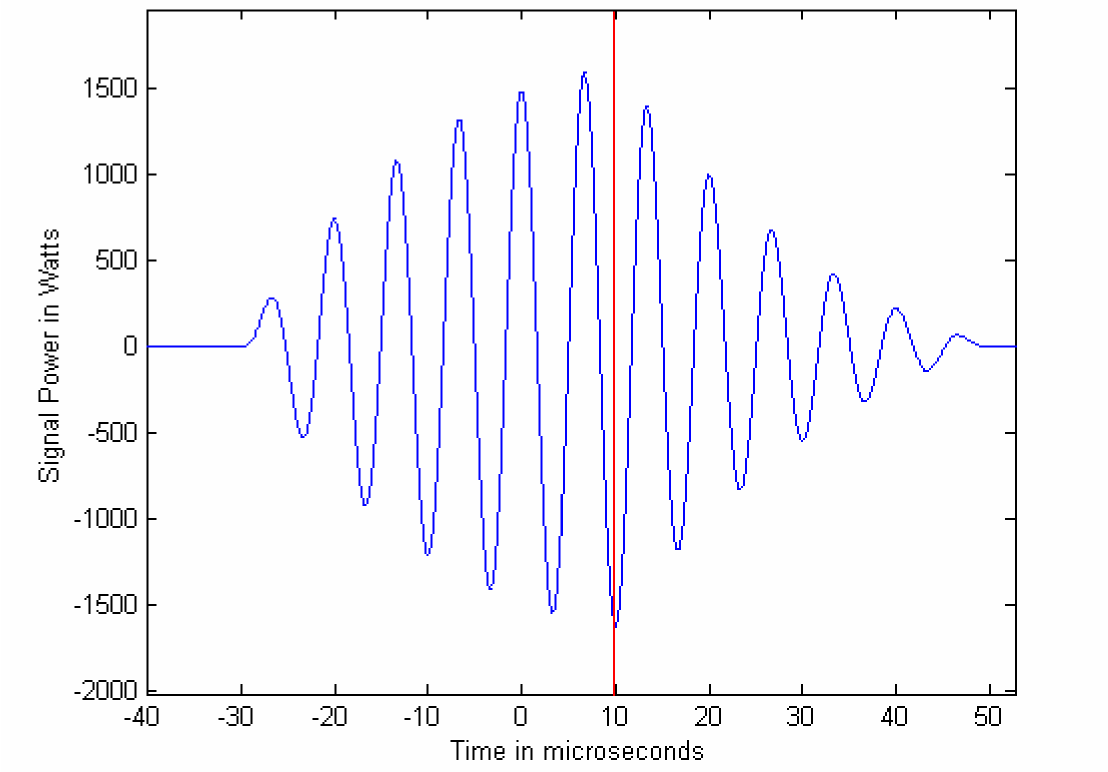

Figure 4.7: Correlation curve for the two sinusoidal signals shown in Figure 4.3. The red line indicates the peak, corresponding to a time difference of 9.98us.

It is obvious that the correlation method performs as well as the filtering method in determining the TDOA in two gated sinusoids with no noise. In addition, if noise is added to the two signals so that the SNR is 8dB, a time difference of 10.025µs is found using the convolution method while the filtering method resulted in a time difference of only 5µs. If the SNR is reduced to 0dB, the convolution method still results in a time difference of 9.99µs. Based on these results, it was concluded that convolution is the more robust and accurate means of determining the TDOA.

While the TDOA is critical in accurately predicting PD location, it is just one step in determining the final position solution. To ascertain the position error resulting from a given TDOA error, a series of positioning simulations were run. First, an improved simulated PD signal was developed in order to more accurately reflect the signal shape observed experimentally. Figure 4.8 shows a representative signal captured from the OA EFPI sensor in the lab. The envelope differs substantially from the simulated signal shown in Figure 4.3 because there is an exponential rise as well as an exponential decay. To correct this discrepancy, the envelope shown in the bottom half of Figure 4.9 was used in the remaining simulations with a 150kHz sinusoid. Figure 4.10 shows all three of the signals for comparison.

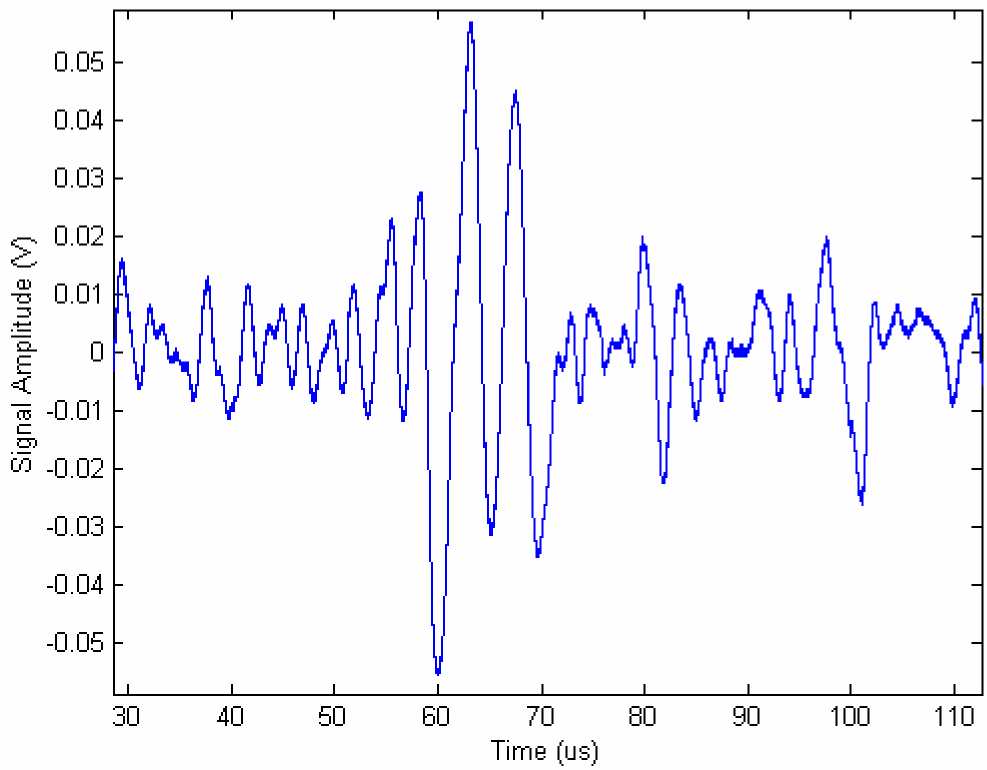

Figure 4.8: Time domain signal captured from the OA EFPI sensor when the sensor is 7cm from the acoustic source.

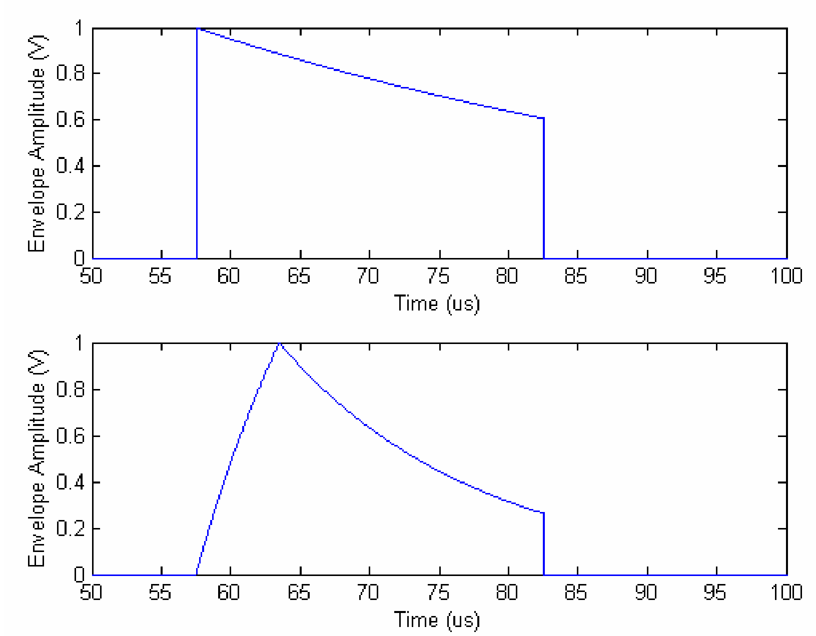

Figure 4.9: Simulated PD signal envelopes used in error simulations. The top graph shows the simple exponentially decaying signal while the bottom graph shows the signals with both an exponential rise and decay.

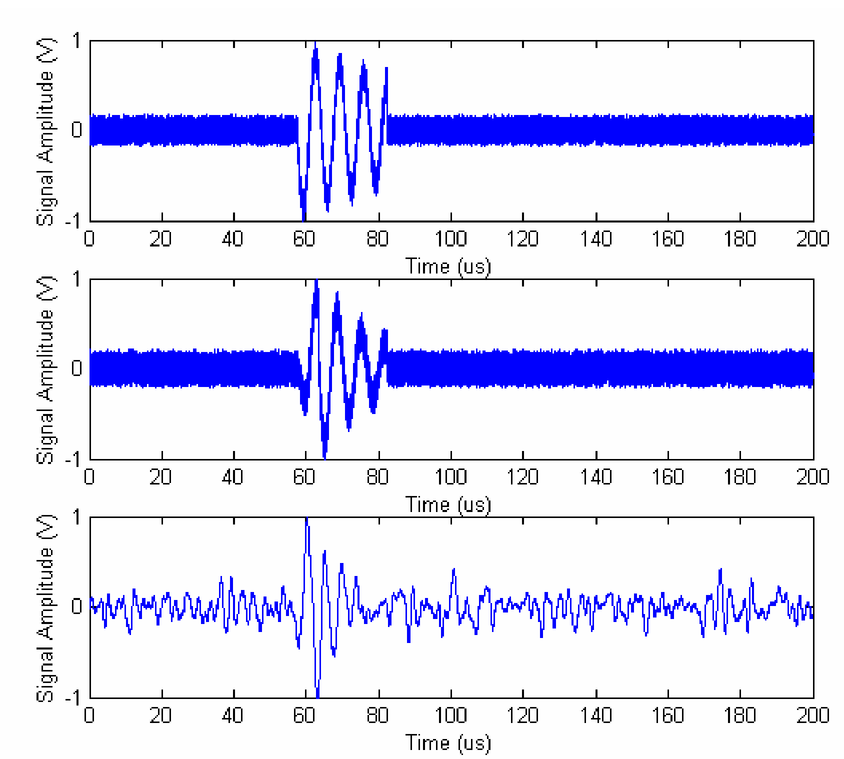

Figure 4.10: Comparison of two simulated signals with a representative data signal from the sensor. The top plot is the exponentially decaying signal with the step edge, the middle plot is a graph of the new simulated signal with both exponential rise and decay and the bottom plot is the data signal shown in Figure 4.8.

The error calculations above assumed fixed signal parameters: ΔT=10μs, f=150kHz, SNR=8dB. However, due to the variable nature of the PD phenomenon, which is explained in Chapter 3, it is important to see how varying the acoustic signal parameters affects the accuracy of the TDOA calculation. The first set of error simulations evaluated the impact of SNR on the time difference error. The SNR of two simulated gated 150kHz signals with a fixed time difference of 67.5μs was varied between 3 and 20dB. As shown in Figure 4.11, the time difference error decays exponentially as the SNR of the two signals increase. To reach the TDOA error associated with the ±5cm position accuracy, which is around 5μs, the SNR of the signals with the above parameters can be as low as 4dB.

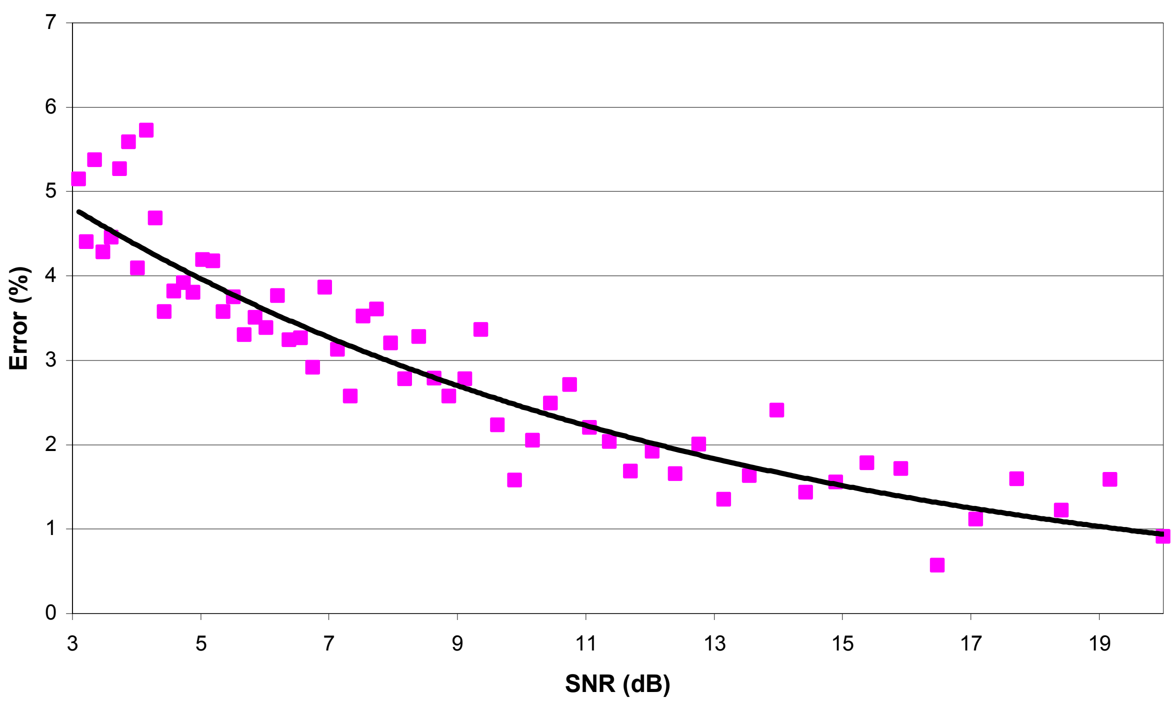

Figure 4.11: Impact of SNR on time difference error produced using the convolution method. The SNR of two simulated signals (f=150kHz, ΔT=67.5μs, double exponential envelope) were varied from 3dB to 20dB. The error in TDOA decreased exponentially as the SNR of the two signals is increased.

The second error study evaluated the effect of the length of the time difference on the resulting accuracy. Changes in time difference correspond to changes in geometrical sensor location. The sinusoidal frequency and SNR were fixed at 150kHz and 14dB and the time difference between the two signals was varied between 5 and 100μs. The simulation was run 100 times and the results averaged to remove the transient effects of the additive white noise. The results shown in Figure 4.12 indicated that the relative error decays exponentially as a function of the time difference. However, the absolute error remains constant at approximately 1.7μs, which is well below the 4.6μs limit.

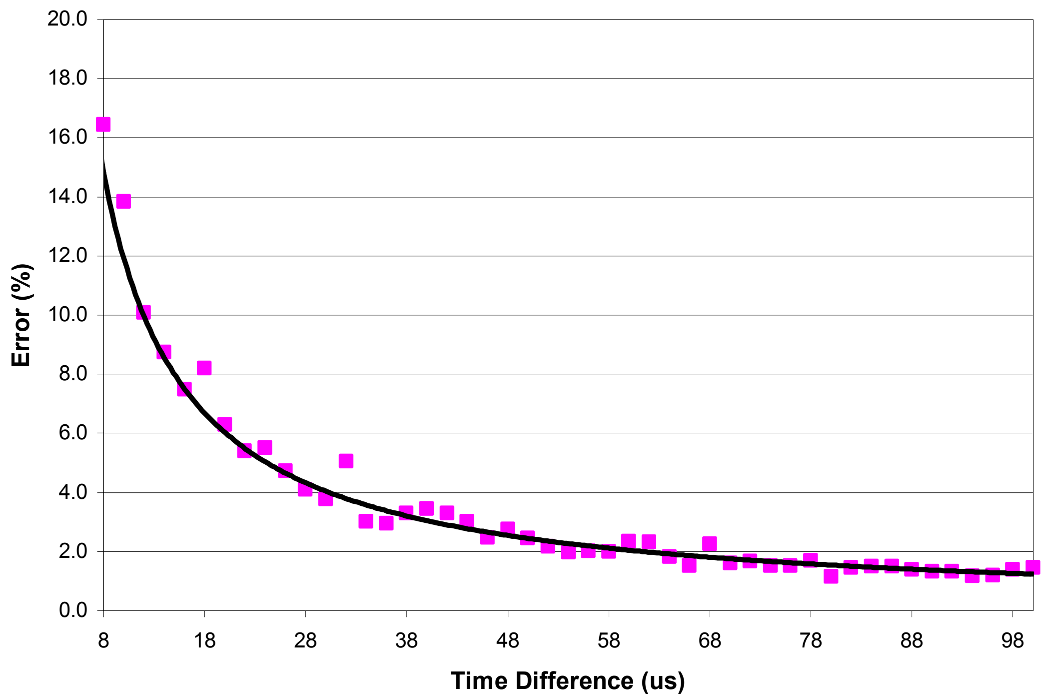

Figure 4.12: Impact of changes in the simulated time difference on relative TDOA error. The time difference between two simulated signals (f=150kHz, SNR=14dB) was varied between 5-100μs. The relative error decays exponentially with increasing time difference, but the absolute TDOA error remains nearly constant at 1.7μs.

The final study investigated the effect of the sinusoidal frequency on the error of the TDOA calculation. This is especially important in PD applications because as stated in Chapter 3, the center frequency of the PD acoustic pulse can vary between 100 and 300 kHz. Therefore, the SNR and time difference between two signals were fixed at 14dB and 67.5μs while the sinusoidal frequency was varied from 100 to 300 kHz. The results of that study are shown in Figure 4.13. The figure shows that the error in the TDOA calculation is fairly constant, at two percent, over the range of 100-300kHz. This error corresponds to a time error of 1.35µs, which is below the threshold for the ±5cm position limit.

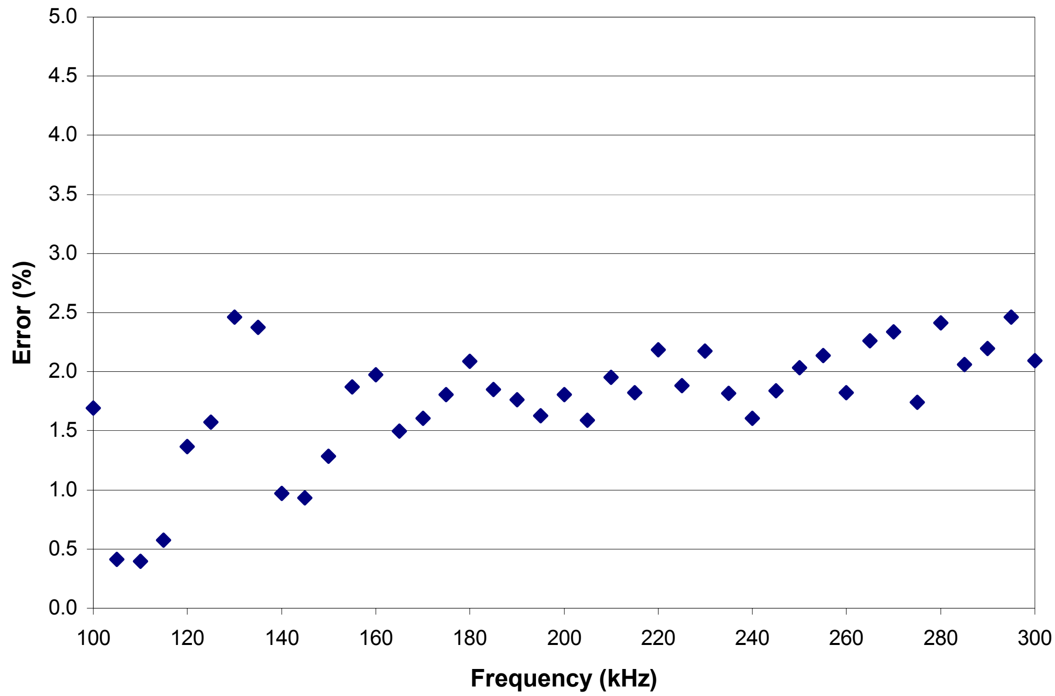

Figure 4.13: Position error as a function of frequency. The plot shows that the TDOA calculated with signals that have an SNR=14dB and a pulse separation of 67.5µs varied between 0.5 and 2.5 percent over the frequency range of interest. This variation corresponds to a maximum time error of 1.35µs, which is less than the threshold of 4.6µs.

Based on these studies, the SNR is the most important source of TDOA error in the convolution method. The resulting position error, given the SNR parameters, can be estimated using Figure 4.11. For example, an SNR of 14dB corresponds to a time error of 1.7µs, which corresponds to a position error of ±8.48mm on each axis. If the SNR is increased to 16dB, then the corresponding time error is around 1µs and the position error is ±5.52mm on each axis.

Section 4.4: Software

The positioning algorithm and the convolution algorithm were implemented in two separate MATLAB m-files. The first m-file, position.m, allows a user to input the coordinates of each of the four sensors in the array and outputs the coordinates of the source. The second m-file, called TDOA.m, reads in the time domain signals from each of the 4 sensors, convolves the signals from sensors 2, 3, and 4 with the signal from sensor 1, finds the peak of the convolution curve, and outputs the corresponding time difference in seconds. Both pieces of code are included in Appendix B. The block diagram in Figure 4.14 illustrates how the two pieces of code work together.

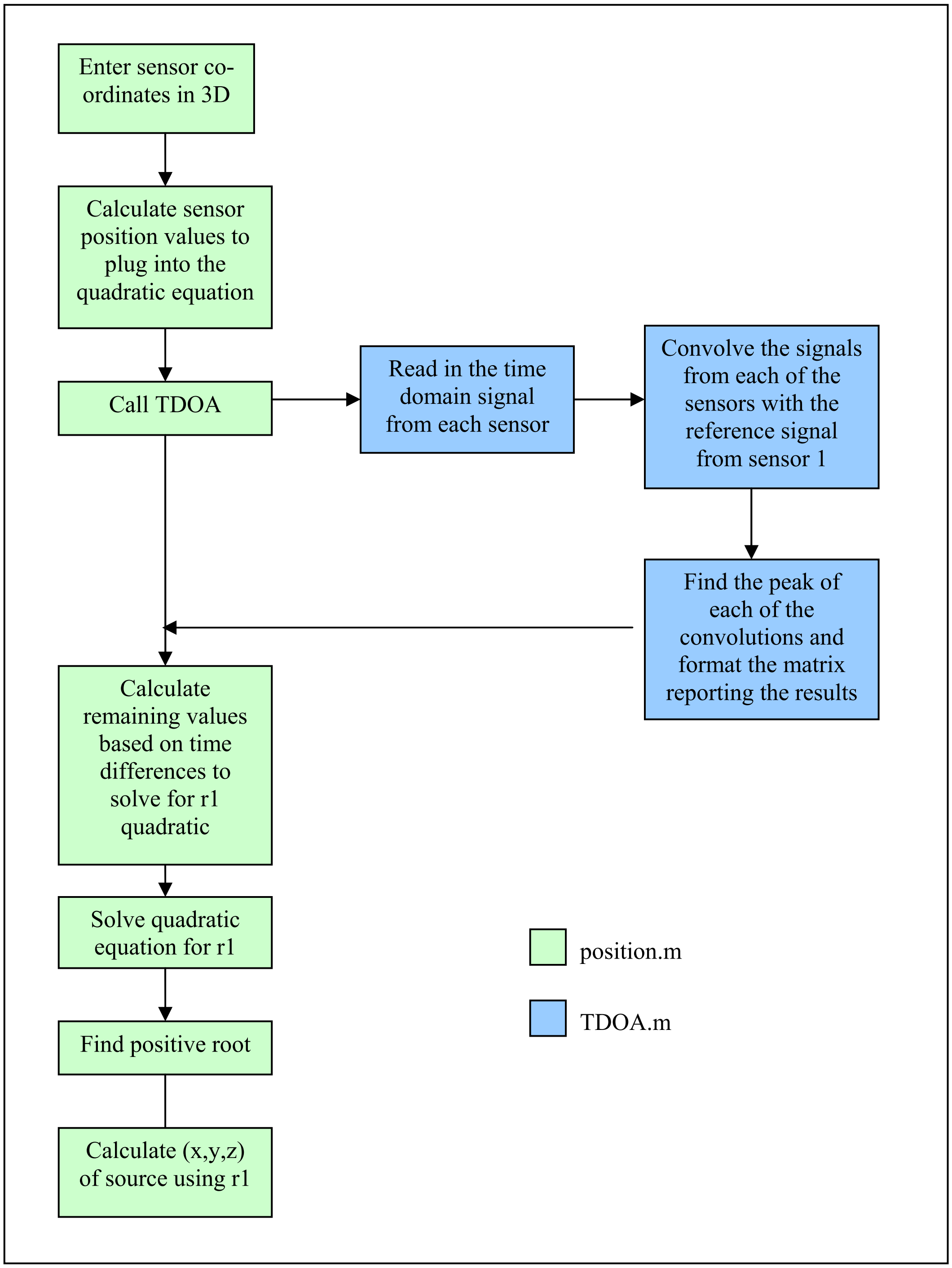

Figure 4.14: Flow chart illustrating how the positioning code was implemented.

Section 4.5: Position Simulation and Experimentation

Section 4.5.1: Simulation Results

The final step in validating the positioning system was to process both simulated and experimental signals. The first step was performed in MATLAB using the two types of simulated signals presented in Section 4.3. Recall that the rising edge on the initial simulated signal was a step while the second simulation had an exponentially increasing leading edge. The second signal was used to evaluate the TDOA error. It is also important at this stage to demonstrate the impact of the pulse shape on the position error.

Table 4.1: Geometry for the simulated position test.

	x-coordinate (mm)	y-coordinate (mm)	z-coordinate (mm)
Sensor 1	4.5	4.5	80
Sensor 2	-15.5	15.5	70
Sensor 3	-7	-12.5	50
Sensor 4	14	-15	20
Source	-11	14	150

Table 4.1 lists the sensor and source locations for the simulation. Given this geometry, the time differences between the sensor signals[§] are 10.08, 23.90, and 41.05μs. The simulated signal parameters were fixed at the following values.

- f=150kHz - This is consistent with the estimated PD center frequency.
- pulse width = 16.5μs – This matches the pulse width measured using the OA sensor.
- Decreasing SNR - Because the acoustic wave spreads and is absorbed while traveling through the transformer tank, the sensor signal will be greatest at the closest sensor and the least at the farthest. To simulate this condition, each of the signals was decreased with respect to the first signal.

[§] Time differences are measured with respect to the closest sensor; in this case, Sensor 1. Therefore, the time differences are between Sensors 1 and 2, Sensors 1 and 3, and Sensors 1 and 4.

Figure 4.15 shows the results of the first test, which was run with no noise in either of the simulated signals to confirm that the positioning software functions as expected and that there is no inherent error in the algorithm when a constant acoustic velocity is assumed. With an infinite SNR, there is no difference between the locations found using the step edged signal and using the exponentially increasing signal.

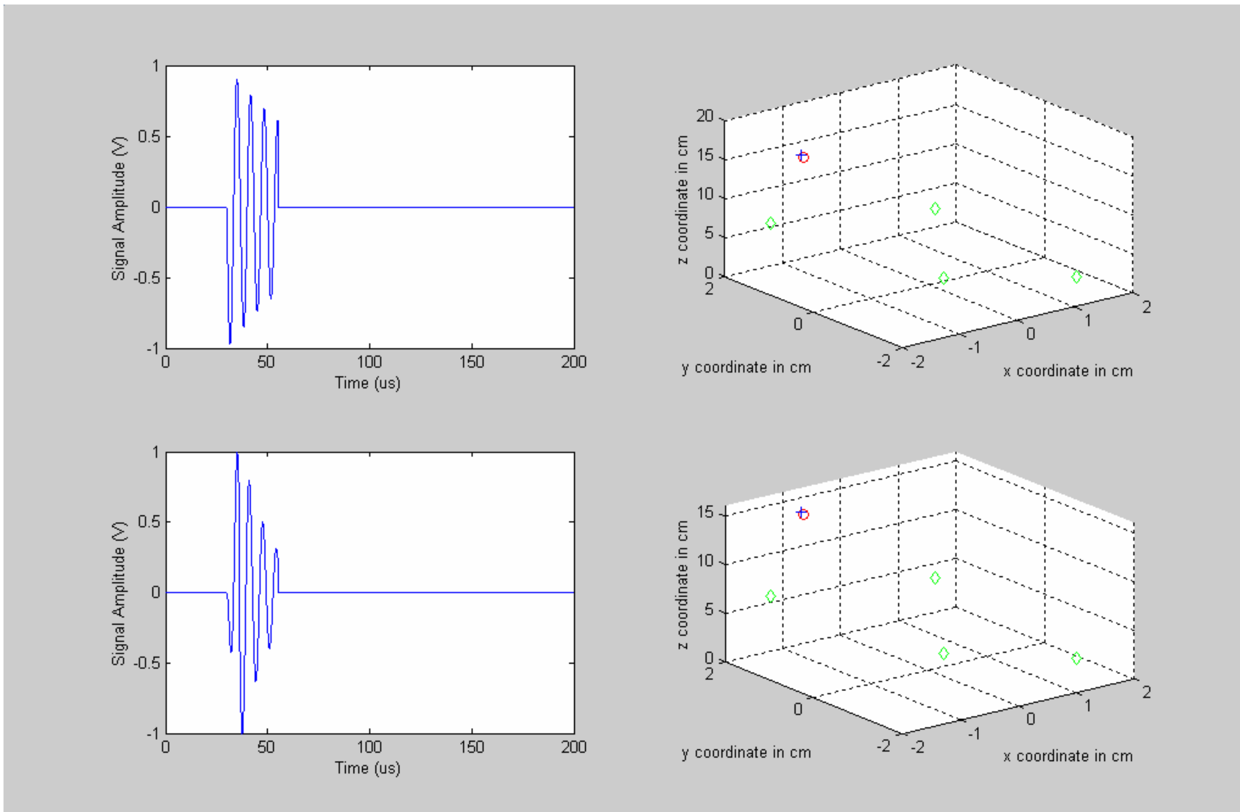

Figure 4.15: Positioning results using noiseless simulated signals with the envelopes shown in Figure 4.9. The plots on the left are representative simulated signals and those on the right are a plot of the calculated sensor locations (green), the source location (red) and the location found by the position code (blue).

The simulations were repeated** using primary signals with an SNR of 7dB††. Figure 4.16 shows the results of the second set of simulations. The results indicate that while an SNR of 7dB is sufficient to reach the accuracy goal using the step rise signal, the exponential rise signal

** The simulation was run 10 different times in order to observe a spread in the PD location data caused by the transient white noise.

†† Because each of the four signals has different amplitudes and the same amount of noise is added to each signal, the SNR for each of the signals is different. However, for each test listed, only the SNR of the strongest signal will be quoted.

does not produce results within the ±5 cm limit on the z-axis. This indicates that the PD signal envelope shape does influence the resulting calculated TDOA. Results based on the double exponential envelope were therefore expected to better coincide with the processed data from laboratory experiments.

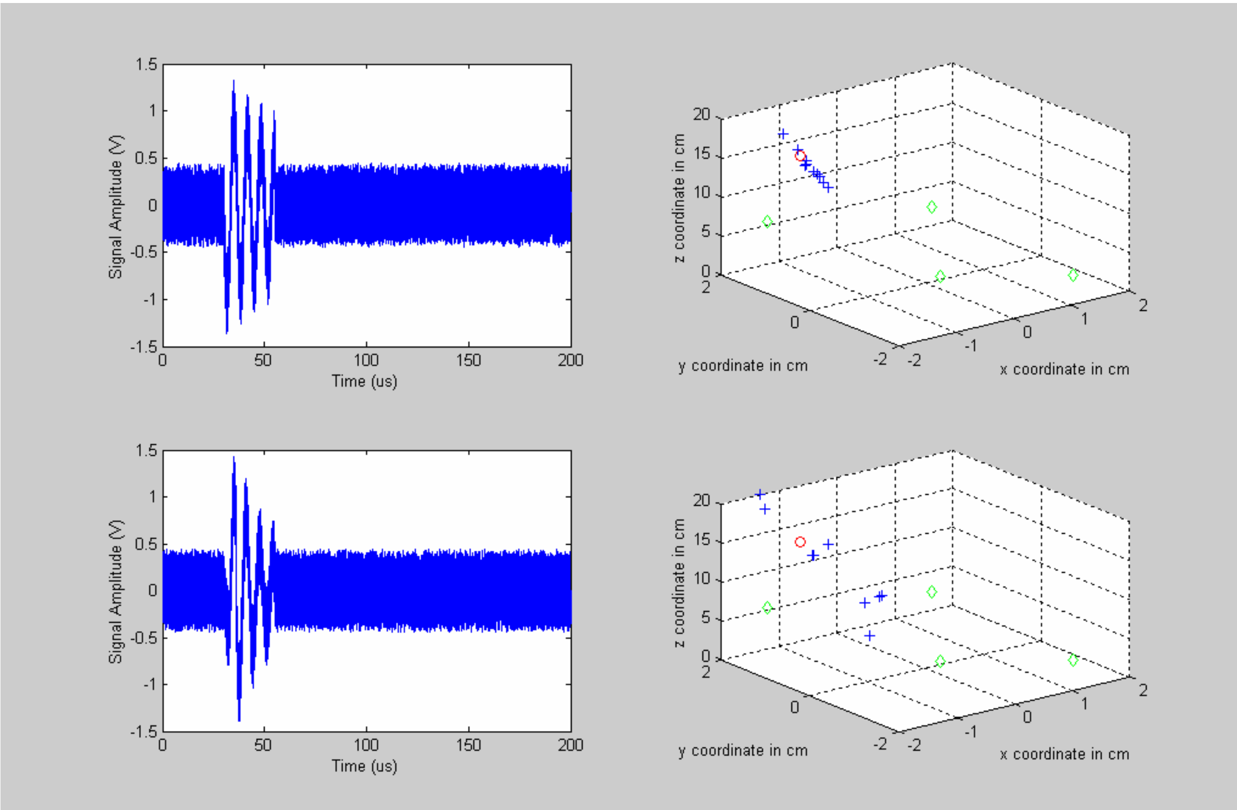

Figure 4.16: Positioning simulation results using signals with additive noise (SNR=7dB). The simulated signal with the step rising edge results in source positions well within the required accuracy. However, the simulated signal more representatives of experimental data does not. The green dots mark the sensor positions, the red dot marks the source location and the blue dots mark the positions found after running the position simulation 10 times.

The objective of the final positioning simulation was to determine the minimum SNR that could result in a position accuracy of ±5cm. The same simulation was repeated with different values of SNR until the error bounds were located. The SNR limit was found to be 14dB and the results of the simulation are shown in Figure 4.17. This final test shows that reliable positioning within the error bounds stated above can be achieved if the signal from the first sensor has an SNR greater than or equal to 14dB.

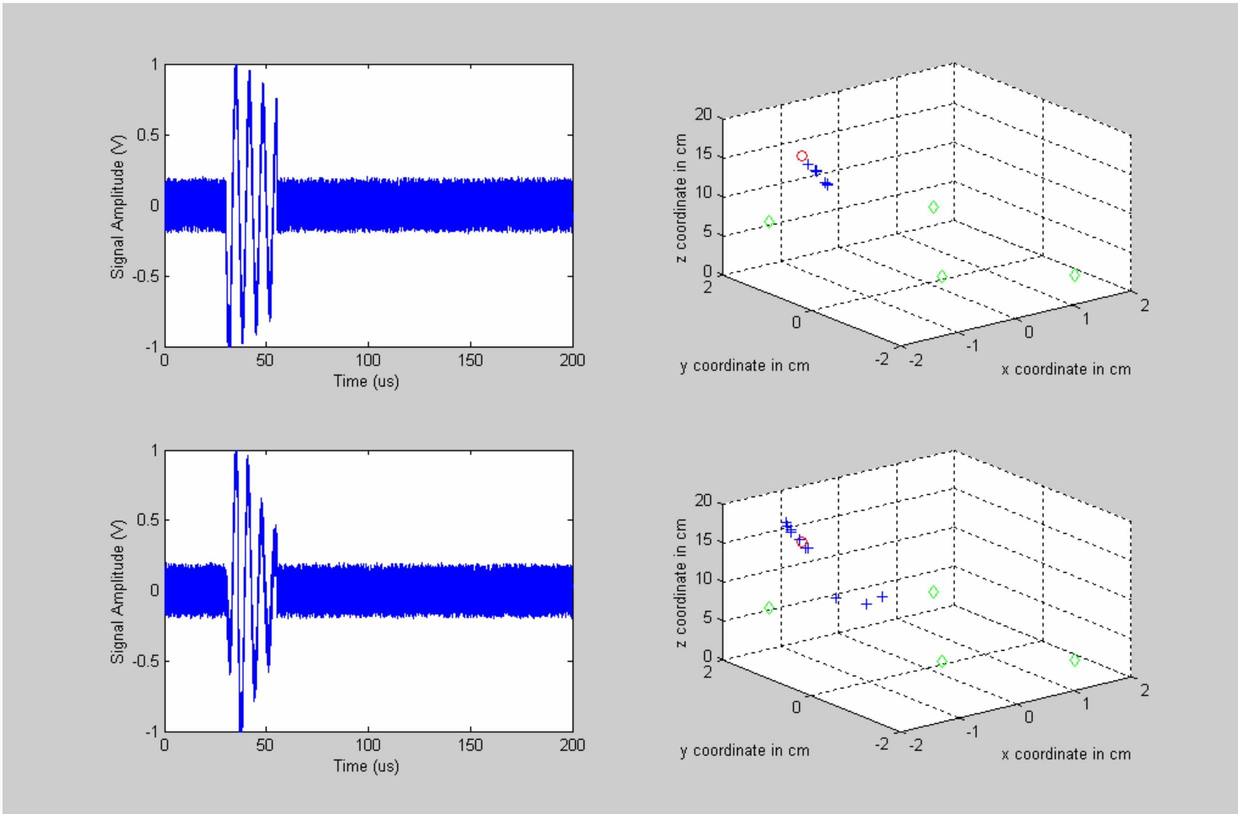

Figure 4.17: Final simulation with an SNR of 14dB. All of the results for the second simulated signal fall within the required ±5cm cube.

Section 4.5.2: Experimental Results

The simulation data indicated that the positioning and TDOA algorithms were capable of delivering a three-dimensional source position to within a 10cm cube if the SNR of the primary signal was at least 14dB and the captured signal has an exponential rising edge. To confirm these conclusions, experimental testing of the whole positioning system was conducted in the laboratory at the Center for Photonics Technology at Virginia Tech. The tests were conducted in a 10-gallon aquarium filled with water. The source configuration was the same as that used in frequency response testing (Chapter 3), where a PZT connected to an electric driver was mounted in a piece of PVC pipe and submerged in the aquarium. The data was then detected by a single sensor moved to different locations within the tank[‡‡] and the signals were collected using an oscilloscope that was externally triggered by the PZT driver. The sensor was held in

[‡‡] Only one sensor was used to guarantee that the frequency content of each of the signals was the same, because different sensors have different frequency responses due to current manufacturing limitations.

place by a sheet of Plexiglas with holes drilled in it so that the senor fit snuggly into place. Figure 4.18 shows pictures of the sensor mounting as well as the experiment setup.

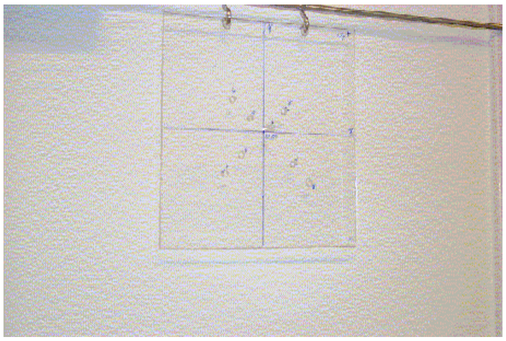

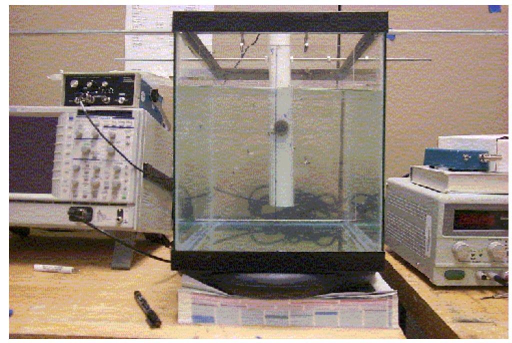

Figure 4.18: Sensor mounting rig and bench top experiment setup. The acoustic PD source was simulated using a PZT submerged in water and the data signal from the sensor was captured digitally using an oscilloscope with a time resolution of 200MS/s. The x-y plane corresponds to the front of the tank, shown in the picture on the right. The z-axis is then parallel to the bench top (going into the picture).

The signals were recorded using a digital oscilloscope with a time resolution of 5ns over a 200μs window from the same positions listed in Table 4.1. At each location, seven data sets were taken to gain a statistically representative spread of location points. Then, the signal to noise ratio of each signal was determined in order to only use signals with SNRs that met the requirements outlined by the SNR error testing and the position simulation. These signals were run in eleven different combinations and results are shown in Figure 4.19 and are listed in Appendix C. The position algorithm performed as expected and all eleven calculated positions fell within the ±5cm limit on all three axes.

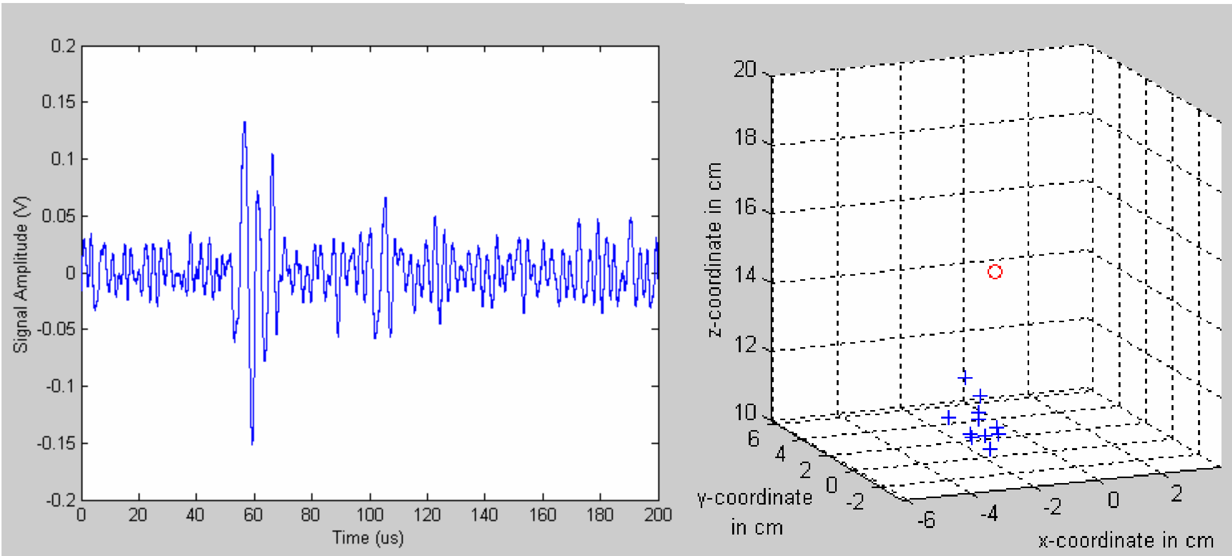

Figure 4.19: Results of the positioning algorithm using experimental data (right) and a representative time domain signal from the OA sensor (left). The position plot is the same size as the ±5cm error cube and all 11 data sets fall within the cube. The sensor positions fall outside of the defined error cube and are not shown in this plot.

Section 4.6: References

[1] P. M. Eleftherion, "Partial Discharge XXI: Acoustic Emission-Based PD Source Location in Transformers," in *IEEE Electrical Insulation Magazine*, vol. 11, 1995, pp. 22-26.

[2] V. Darley, "Partial Discharges within Power Transformers and the Use of Ultrasonic Techniques in Their Location," presented at IEE Colloquium on Assessment of Degradation Within Transformer Insulation Systems, London, U.K., 1991.

[3] E. G. F.H. Kreuger, and A. Krivda, "Classification of Partial Discharges," *IEEE Transactions on Electrical Insulation*, vol. 28, pp. 917-931, 1993.

[4] Y. H. G. Wang, and Y. Li, "Study on pulse current of typical PD models in power transformer," presented at International Symposium on Electrical Insulating Materials (ISEIM 2001), 2001.

[5] Y. T. a. H. Chan, K.C., "A Simple and Efficient Estimator for Hyperbolic Location," *IEEE Transactions on Signal Processing*, vol. 42, pp. 1905-1915, 1994.

Chapter 5: Conclusions

Partial discharge detection and location in high voltage transformers is an essential diagnostic tool for monitoring the state of health of electrical insulators within the transformer. The insulation breaks down over time due to mechanical and electrical stresses and if the insulation damage becomes severe, the device could suffer a catastrophic failure that not only causes an unscheduled service outage, but also causes damage to surrounding equipment and threatens the safety of onsite personnel. Partial discharges are one symptom of insulation breakdown because the developing faults in the insulation cause a local build up of electrical charge, which is then dissipated in the form of an electrical and mechanical pulse of energy. In addition, PDs make insulation damage worse because the event adds more electrical and mechanical stress to the developing flaw. Therefore, accurate detection and positioning is required to maintain these devices and limit the amount of diagnostic and repair time required.

This thesis presents an acoustic detection and location system consisting of an array of optical acoustic sensors based on extrinsic Fabry-Perot interferometry. The sensors, which are small in size and chemically and electrically inert, are capable of operating within the tank of the transformer without changing the functionality of the transformer. This capability, which is not available in any commercial PD detection equipment, allows the sensor to measure higher signal amplitudes as well to be immune from multipath errors caused by the varying acoustic speeds of the pulse through different parts of the transformer.

Section 5.1: Results

Simulated and experimental results were presented to verify that the PD detection and location system would function within the specified parameters. The first step in the project was to determine if the OA sensor was capable of detecting a PD acoustic signal. Previous PD research has shown that that center frequency of an acoustic PD pulse varies between 100 and 300 kHz. Using experimental and simulation data, it was demonstrated that the frequency response of an extrinsic Fabry-Perot interferometric (EFPI) fiber optic sensor with a 150μm thick diaphragm is flat over a range of 150 kHz with a center frequency of 150 kHz, which matches the center frequency of a PD acoustic pulse.

Once it was confirmed that the sensor could detect an acoustic PD signal, the positioning system was designed. The algorithm used in this system is based on solving hyperbolic range equations dependent on the time difference of arrival of an acoustic signal at two sensors in an array. If four sensors are used and a constant acoustic velocity is assumed, then the equations can be solved exactly with no inherent error due to the algorithm. Therefore the only sources of error in the position algorithm are derived from the accuracy limits of the measured time difference and the location of the sensors. To minimize the time difference error, both convolution and high pass filtering were considered for the time difference algorithm, but the convolution method proved to be more robust in the presence of noise. In order to set limits on acceptable signal characteristics for reliable positioning, the impact of different signal parameters on the time difference error was evaluated. The signal shape was first optimized to better reflect experimental data characteristics by incorporating an exponential rising edge, and then the signal to noise ratio (SNR), time difference, and frequency of the signal were varied. The SNR of the signal has the greatest effect on the accuracy of the time difference calculation. The results of this study were used to estimate the position accuracy corresponding to given signal parameters.

The first full test of the positioning code consisted of using simulated signals with varied SNRs to determine if the error bound of ±5cm on each axis could be achieved. It was concluded that the accuracy goal could be achieved if the SNR of the primary signal was 14dB or greater. The final step in validating the positioning system was to test the TDOA and positioning code using experimental data. For signals that meeting the SNR requirement, the error bound was achieved and the positioning system based on the EFPI fiber optic acoustic sensor was validated.

Section 5.2: Future Work

The ultimate goal of this project is to design and implement a PD detection and location system in a commercial power environment. The work presented in this thesis represents the preliminary studies necessary to achieve that goal and demonstrates the feasibility of the approach. Before this system can be implemented in the field, additional studies will be required. First and foremost is further investigation of the PD phenomenon itself. As stated in Chapter 3, there is little agreement in the literature on the characteristics of acoustic PD pulses including the frequency content and pulse duration. This ambiguity makes it extremely difficult to optimize sensor characteristics for detecting the phenomenon.

The second area of further study is the angular dependence of the sensor frequency response. The frequency response testing reported in Chapter 3 is based on a signal with normal incidence on the sensor diaphragm. However, in an HVT there is no guarantee that the acoustic wave will be incident perpendicular to the surface of the sensor. In fact, in the laboratory positioning testing described in Chapter 4 the sensors were not limited to normal incidence. A finite element analysis (FEA) of the diaphragm when loaded with a viscous fluid on one side would provide valuable insight into the functionality of the sensor and could be used to increase the sensitivity in future designs. In addition, knowing the angular dependence of the frequency response would allow an array frequency response to be constructed and the effective aperture of the sensor array could be calculated for specific sensor separations. The FEA model would also have to be validated in a laboratory environment; much like the frequency response was validated in this thesis.

The third area of future research is an investigation of the effect of obstructions on the propagation of the acoustic wave within the transformer tank. Because of the inhomogeneous nature of the tank, it is important to understand how signals are attenuated and diffracted as they pass through the mineral oil in the HVT. Results of a study of this kind could be used to determine sensor placement within the tank and combined with the angular frequency dependence, an efficient sensor layout could be designed to offer the largest coverage of the HVT interior with the least number of sensors.

Two final studies, noise suppression and field testing, are required before the system can be deployed in the field. Research in noise suppression, specifically using the technique of wavelet transforms, would improve the signal to noise ratio of the measured PD signal and therefore would improve the accuracy of the positioning system, as described in Chapter 4. Wavelet transforms have been used in past work to denoise a PD signal, but this technique has not been used in conjunction with a PD positioning system. The final area of future study is field testing the whole system in a real world HVT. The true accuracy of the system as well as required improvements and optimization can be determined by operating the system under real conditions. The data from such tests would then allow a commercial company to take on the manufacture and installation of this system in HVTs.

Appendix A: Correlation and TDOA

In Chapter 4, Section 3.2, it is stated that the time difference between two signals can be found by finding the peak of the correlation curve. A simulation using two square pulses was run to demonstrate this point. The square pulses were created using arrays of ones and zeros that had been offset by 7 units of time. When the tow signals were convolved, using the conv() function in MATLAB, the resulting peak of the convolution occurred at 7 time units. The square wave signals and the convolution peak are shown in Figure A.1.

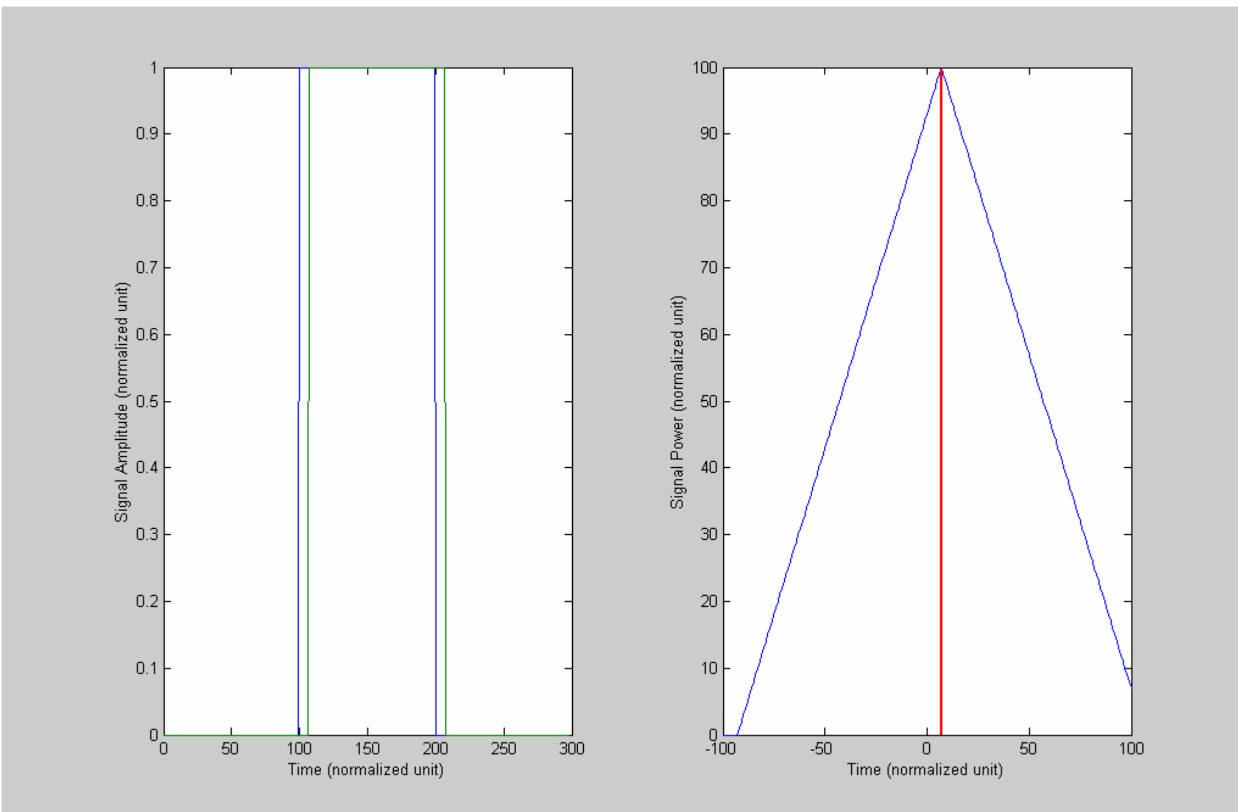

Figure A.1: Two offset square waves (left) and their convolution curve(right). The peak of the convolution occurs at 7 time units, which is the same as the space between the two square waves.

When additive white noise is noise is added to the two square waves, the convolution peak changes. The result of the convolution to two noisy square waves is shown in Figure A.2. In the presence of noise, the convolution still produces a time difference of 7 time units. This demonstration shows that convolution can be used to determine the time difference between two identical signals.

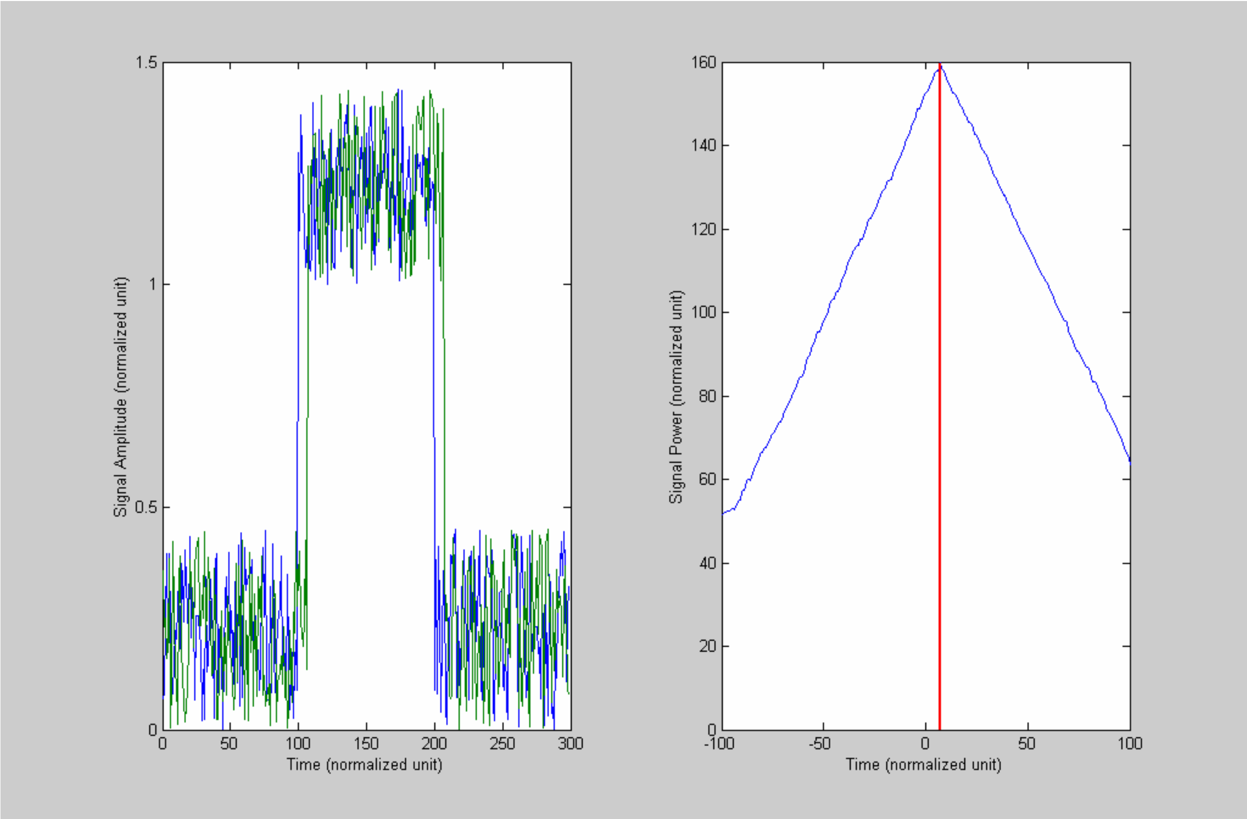

Figure A.2: Convolution of two noisy square waves. The signals each have a SNR of 7dB and the resulting peak of the convolution curve occurs at 7, which is the correct value of time separation.

Appendix B: MATLAB Code

Section B.1: Positioning Software

```
function solution=position_final(m1,m2,m3,m4,D)


%%%%%%%%%%%%%%%%%%%%%%%%%%%%%%%%%%%%%%%%%%%%%%%%%%%%%%%%%%%
% position_final.m                                                                          %
%                                                                                           %
% January 22, 2003                                                                          %
%                                                                                           %
% This script takes reads in the four acoustic signals from an outside function and         %
% returns the position of the "source" based on time difference of arrival.  This script    %
% calls TDOA, which correlates the recorded time signals and outputs the time difference    %
% of arrival to each of the sensors, based on the reference sensor.                         %
%                                                                                           %
%                                                                                           %
% Written by Alison Lazarevich                                                              %
% Center for Photonics Technology, Virginia Tech                                            %
%%%%%%%%%%%%%%%%%%%%%%%%%%%%%%%%%%%%%%%%%%%%%%%%%%%%%%%%%%%

%Define Constants

%Speed of Sound in the medium
speed_of_sound = 1480;

%Input co-ordinates of the sensors

sensor1 = [4.5 4.5 80].*10^-3;
sensor2 = [-15.5 15.5 70].*10^-3;
sensor3 = [-7 -12.5 50].*10^-3;
sensor4 = [14 -15 20].*10^-3;

%Compute the co-ordinate differences

delta_x=[sensor2(1)-sensor1(1) sensor3(1)-sensor1(1) sensor4(1)-sensor1(1)];
delta_y=[sensor2(2)-sensor1(2) sensor3(2)-sensor1(2) sensor4(2)-sensor1(2)];
delta_z=[sensor2(3)-sensor1(3) sensor3(3)-sensor1(3) sensor4(3)-sensor1(3)];

%Compute K values

K1= sensor1(1)^2 + sensor1(2)^2 + sensor1(3)^2;
K2= sensor2(1)^2 + sensor2(2)^2 + sensor2(3)^2;
K3= sensor3(1)^2 + sensor3(2)^2 + sensor3(3)^2;
K4= sensor4(1)^2 + sensor4(2)^2 + sensor4(3)^2;

%Call TDOA to get time differences

T= TDOA(m1,m2,m3,m4);

%Define range differences
```

```
delta_r = speed_of_sound.* T;

%Define Constants to solve r1 quadradic
x21 = delta_x(1);
x31 = delta_x(2);
x41 = delta_x(3);
y21 = delta_y(1);
y31 = delta_y(2);
y41 = delta_y(3);
z21 = delta_z(1);
z31 = delta_z(2);
z41 = delta_z(3);

r21=delta_r(1);
r31=delta_r(2);
r41=delta_r(3);

a = r21^2 - K2 + K1;
b = r31^2 - K3 + K1;
c = r41^2 - K4 + K1;

x1 = sensor1(1);
y1 = sensor1(2);
z1 = sensor1(3);


%Form quadradic in r1 and solve for the positive root
%Co-efficient of squared term
squared_term = ((-(x31*z41-z31*x41)/(x21*y31*z41-x21*z31*y41-x31*y21*z41+x31*z21*y41+x41*y21*z31-
x41*z21*y31)*r21+(x21*z41-z21*x41)/(x21*y31*z41-x21*z31*y41-x31*y21*z41+x31*z21*y41+x41*y21*z31-
x41*z21*y31)*r31-(x21*z31-z21*x31)/(x21*y31*z41-x21*z31*y41-x31*y21*z41+x31*z21*y41+x41*y21*z31-
x41*z21*y31)*r41)^2+((y31*z41-z31*y41)/(x21*y31*z41-x21*z31*y41-
x31*y21*z41+x31*z21*y41+x41*y21*z31-x41*z21*y31)*r21+(-y21*z41+z21*y41)/(x21*y31*z41-x21*z31*y41-
x31*y21*z41+x31*z21*y41+x41*y21*z31-x41*z21*y31)*r31-(-y21*z31+z21*y31)/(x21*y31*z41-x21*z31*y41-
x31*y21*z41+x31*z21*y41+x41*y21*z31-x41*z21*y31)*r41)^2+(-(-x31*y41+y31*x41)/(x21*y31*z41-
x21*z31*y41-x31*y21*z41+x31*z21*y41+x41*y21*z31-x41*z21*y31)*r21-(x21*y41-y21*x41)/(x21*y31*z41-
x21*z31*y41-x31*y21*z41+x31*z21*y41+x41*y21*z31-x41*z21*y31)*r31+(x21*y31-y21*x31)/(x21*y31*z41-
x21*z31*y41-x31*y21*z41+x31*z21*y41+x41*y21*z31-x41*z21*y31)*r41)^2-1);

%Co-efficient of single term
single_term = (2*(x1+1/2*(y31*z41-z31*y41)/(x21*y31*z41-x21*z31*y41-
x31*y21*z41+x31*z21*y41+x41*y21*z31-x41*z21*y31)*a+1/2*(-y21*z41+z21*y41)/(x21*y31*z41-
x21*z31*y41-x31*y21*z41+x31*z21*y41+x41*y21*z31-x41*z21*y31)*b-1/2*(-
y21*z31+z21*y31)/(x21*y31*z41-x21*z31*y41-x31*y21*z41+x31*z21*y41+x41*y21*z31-
x41*z21*y31)*c)*((y31*z41-z31*y41)/(x21*y31*z41-x21*z31*y41-x31*y21*z41+x31*z21*y41+x41*y21*z31-
x41*z21*y31)*r21+(-y21*z41+z21*y41)/(x21*y31*z41-x21*z31*y41-x31*y21*z41+x31*z21*y41+x41*y21*z31-
x41*z21*y31)*r31-(-y21*z31+z21*y31)/(x21*y31*z41-x21*z31*y41-x31*y21*z41+x31*z21*y41+x41*y21*z31-
x41*z21*y31)*r41)+2*(y1-1/2*(x31*z41-z31*x41)/(x21*y31*z41-x21*z31*y41-
x31*y21*z41+x31*z21*y41+x41*y21*z31-x41*z21*y31)*a+1/2*(x21*z41-z21*x41)/(x21*y31*z41-
x21*z31*y41-x31*y21*z41+x31*z21*y41+x41*y21*z31-x41*z21*y31)*b-1/2*(x21*z31-z21*x31)/(x21*y31*z41-
x21*z31*y41-x31*y21*z41+x31*z21*y41+x41*y21*z31-x41*z21*y31)*c)*(-(x31*z41-z31*x41)/(x21*y31*z41-
x21*z31*y41-x31*y21*z41+x31*z21*y41+x41*y21*z31-x41*z21*y31)*r21+(x21*z41-z21*x41)/(x21*y31*z41-
x21*z31*y41-x31*y21*z41+x31*z21*y41+x41*y21*z31-x41*z21*y31)*r31-(x21*z31-z21*x31)/(x21*y31*z41-
x21*z31*y41-x31*y21*z41+x31*z21*y41+x41*y21*z31-x41*z21*y31)*r41)+2*(z1-1/2*(-
x31*y41+y31*x41)/(x21*y31*z41-x21*z31*y41-x31*y21*z41+x31*z21*y41+x41*y21*z31-x41*z21*y31)*a-
1/2*(x21*y41-y21*x41)/(x21*y31*z41-x21*z31*y41-x31*y21*z41+x31*z21*y41+x41*y21*z31-
```

```
x41*z21*y31)*b+1/2*(x21*y31-y21*x31)/(x21*y31*z41-x21*z31*y41-
x31*y21*z41+x31*z21*y41+x41*y21*z31-x41*z21*y31)*c)*(-(-x31*y41+y31*x41)/(x21*y31*z41-x21*z31*y41-
x31*y21*z41+x31*z21*y41+x41*y21*z31-x41*z21*y31)*r21-(x21*y41-y21*x41)/(x21*y31*z41-x21*z31*y41-
x31*y21*z41+x31*z21*y41+x41*y21*z31-x41*z21*y31)*r31+(x21*y31-y21*x31)/(x21*y31*z41-x21*z31*y41-
x31*y21*z41+x31*z21*y41+x41*y21*z31-x41*z21*y31)*r41));

%Constant term
const_term = (x1+1/2*(y31*z41-z31*y41)/(x21*y31*z41-x21*z31*y41-
x31*y21*z41+x31*z21*y41+x41*y21*z31-x41*z21*y31)*a+1/2*(-y21*z41+z21*y41)/(x21*y31*z41-
x21*z31*y41-x31*y21*z41+x31*z21*y41+x41*y21*z31-x41*z21*y31)*b-1/2*(-
y21*z31+z21*y31)/(x21*y31*z41-x21*z31*y41-x31*y21*z41+x31*z21*y41+x41*y21*z31-
x41*z21*y31)*c)^2+(z1-1/2*(-x31*y41+y31*x41)/(x21*y31*z41-x21*z31*y41-
x31*y21*z41+x31*z21*y41+x41*y21*z31-x41*z21*y31)*a-1/2*(x21*y41-y21*x41)/(x21*y31*z41-x21*z31*y41-
x31*y21*z41+x31*z21*y41+x41*y21*z31-x41*z21*y31)*b+1/2*(x21*y31-y21*x31)/(x21*y31*z41-
x21*z31*y41-x31*y21*z41+x31*z21*y41+x41*y21*z31-x41*z21*y31)*c)^2+(y1-1/2*(x31*z41-
z31*x41)/(x21*y31*z41-x21*z31*y41-x31*y21*z41+x31*z21*y41+x41*y21*z31-
x41*z21*y31)*a+1/2*(x21*z41-z21*x41)/(x21*y31*z41-x21*z31*y41-
x31*y21*z41+x31*z21*y41+x41*y21*z31-x41*z21*y31)*b-1/2*(x21*z31-z21*x31)/(x21*y31*z41-x21*z31*y41-
x31*y21*z41+x31*z21*y41+x41*y21*z31-x41*z21*y31)*c)^2;

first_root = (-single_term + sqrt(single_term^2-4*squared_term*const_term))/(2*squared_term);
second_root = (-single_term - sqrt(single_term^2-4*squared_term*const_term))/(2*squared_term);

%Set imaginary part of the roots to zeros if they are complex
first_root = real(first_root);
second_root = real(second_root);

%Define Matrix for equation solve, find right root to plug back in, solve for x,y,z

%Define matrises for solution

   A = [x21 y21 z21;x31 y31 z31; x41 y41 z41];
   B = [a;b;c];

%Chose positive root
if first_root>0 & second_root>0

   r1 = first_root;
   r1b = second_root;
   stuff=1

   %Find solution

   solution1 = abs(-(A^-1)*(r1.*delta_r'+ 0.5.*B));
   solution2 = abs(-(A^-1)*(r1b.*delta_r'+ 0.5.*B));

   if abs(solution1(1))> 20*10^-3
     solution = solution2;
   else
     solution=solution1;
   end


elseif first_root<0

  r1 = abs(second_root);
```

```
  stuff=2
  %Find solution

  solution = -(A^-1)*(r1.*delta_r'+ 0.5.*B);

else
  r1 = abs(first_root);
  stuff=3
  %Find solution

  solution = -(A^-1)*(r1.*delta_r'+ 0.5.*B);

end
```

Section B.2: TDOA Software

```
function [T] = TDOA(m1,m2,m3,m4)

%%%%%%%%%%%%%%%%%%%%%%%%%%%%%%%%%%%%%%%%%%%%%%%%%%%%%%%%%%%%%%
% TDOA.m                                                      %
%                                                             %
% February 24, 2003                                           %
% This script, called by position_final.m, takes the          %
% acoustic signals m1,m2,m3,m4 and finds the time             %
% between them by cross-convolving the signals.               %
% The resulting time difference is then passed out            %
% in the form of a row matrix and each element is             %
% in microseconds.                                            %
%                                                             %
% Written by Alison Lazarevich                                %
% Center for Photonics Techonology, Virginia Tech             %
%%%%%%%%%%%%%%%%%%%%%%%%%%%%%%%%%%%%%%%%%%%%%%%%%%%%%%%%%%%%%%

signal1 = load(m1);
signal1 = -[signal1'];
signal2 = load(m2);
signal2 = [signal2'];
signal3 = load(m3);
signal3 = [signal3'];
signal4 = load(m4);
signal4 = [signal4'];

h1=conv(signal1,signal2);
h2=conv(signal1,signal3);
h3=conv(signal1,signal4);

g1=conv(signal1,signal1);

[l,m]=max(abs(h1));
[n,o]=max(abs(h2));
[p,q]=max(abs(h3));

[a,b]=max(abs(g1));

t21=abs(m-b).*0.005;
t31=abs(o-b).*0.005;
t41=abs(q-b).*0.005;

T=[t21 t31 t41].*10^-6;
```

Appendix C: Position Results

The experimental data analyzed for this thesis resulted in the positions listed below.

Table C.1: Data points from Figure 4.19.

	X coordinate (cm)	Y coordinate (cm)	Z coordinate (cm)
Source	-1.1	1.4	15
Data Set 1	-2.0033	0.3693	11.7160
Data Set 2	-1.5085	1.1372	10.3269
Data Set 3	-3.8780	-1.8405	11.7732
Data Set 4	-2.0604	1.3625	11.9919
Data Set 5	-3.1961	-2.3759	11.9645
Data Set 6	-2.6997	-2.6163	11.5515
Data Set 7	-3.2479	-2.0773	11.1975
Data Set 8	-1.3463	0.5795	10.4796
Data Set 9	-1.7406	1.1147	10.8387
Data Set 10	-3.3434	-2.1659	11.3237
Data Set 11	-2.8103	-2.3275	10.8570

Vita

Alison K. Lazarevich was born in Sterling, Va. She received her B.S. degree in Electrical Engineering with an emphasis in Communications and minor in Mathematics from Virginia Tech in December 2001. During her time at Virginia Tech, she was hired as a co-op student for the Central Intelligence Agency in Langley, Va. and worked on both RF and optical communications systems. In addition to her academic endeavors, she is an active member of the Virginia Tech Student Chapter of the IEEE and has organized several events including a research lab showcase aimed at getting undergraduate students involved in research programs. She joined the Center for Photonics Technology at Virginia Tech in May of 2002 where she has worked exclusively on partial discharge detection and location using optical sensors. Her research interests include fiber optic device simulation and testing, electromagnetic propagation simulation and optical system design.